



저작자표시-비영리-변경금지 2.0 대한민국

이용자는 아래의 조건을 따르는 경우에 한하여 자유롭게

- 이 저작물을 복제, 배포, 전송, 전시, 공연 및 방송할 수 있습니다.

다음과 같은 조건을 따라야 합니다:



저작자표시. 귀하는 원저작자를 표시하여야 합니다.



비영리. 귀하는 이 저작물을 영리 목적으로 이용할 수 없습니다.



변경금지. 귀하는 이 저작물을 개작, 변형 또는 가공할 수 없습니다.

- 귀하는, 이 저작물의 재이용이나 배포의 경우, 이 저작물에 적용된 이용허락조건을 명확하게 나타내어야 합니다.
- 저작권자로부터 별도의 허가를 받으면 이러한 조건들은 적용되지 않습니다.

저작권법에 따른 이용자의 권리는 위의 내용에 의하여 영향을 받지 않습니다.

이것은 [이용허락규약\(Legal Code\)](#)을 이해하기 쉽게 요약한 것입니다.

[Disclaimer](#)

Master Thesis

**Precision Patterning of Superhydrophobic-  
Superhydrophilic Microdroplet Arrays:  
Towards On-Demand Sustainable  
Manufacturing of Functional Materials**

University of Ulsan

School of Mechanical Engineering

**MOHAMMAD IMRAN BAPPY**

July 2024

초소수성-초소수성 마이크로 액적 어레이의 정밀패턴화: 기능성 소재의  
온디맨드 지속가능한 제조를 향한 연구

# **Precision Patterning of Superhydrophobic- Superhydrophilic Microdroplet Arrays: Towards On-Demand Sustainable Manufacturing of Functional Materials**

지도교수 천두만

이논문을 공학석사 학위 논문으로 제출함

2024 년 07 월

울산대학교 대학원 기계공학과

**MOHAMMAD IMRAN BAPPY**

**Precision Patterning of Superhydrophobic-  
Superhydrophilic Microdroplet Arrays: Towards  
On-Demand Sustainable Manufacturing of  
Functional Materials**

A Thesis

Submitted to the School of Mechanical Engineering and the Graduate  
School of the University of Ulsan, Republic of Korea in partial  
fulfillment of the requirements for *the degree of Master of Science in  
Mechanical Engineering*

By

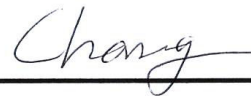
**MOHAMMAD IMRAN BAPPY**

Master's Thesis

**This certifies the thesis approval of Mohammad Imran Bappy**

**Thesis Committee Chairman**

**Professor Kyoungsik Chang**



---

**Thesis Committee Member**

**Professor BoHung Kim**



---

**Thesis Committee Member**

**Professor Doo-Man Chun**



---



# TABLE OF CONTENT

ACKNOWLEDGEMENT .....	i
ABSTRACT .....	ii
LIST OF TABLES .....	iii
LIST OF FIGURES .....	iii
LIST OF ABBREVIATIONS.....	vi
CHAPTER 1 INTRODUCTION .....	1
1.1. Introduction to Surface Wettability.....	1
1.2. Droplet Microarray.....	3
1.3. Previous Trends In Droplet Microarray Research .....	5
1.4. Objectives of Our Research.....	6
CHAPTER 2 EXPERIMENT .....	8
2.1. Materials .....	8
2.2. Laser Texturing System .....	8
2.3. Fabrication Process.....	10
2.4. Material characterization.....	15
CHAPTER 3 RESULTS AND DISCUSSION.....	16
3.1. Effect of the Laser Processing Parameters for Superhydrophobic Fabrication .....	16
3.2. Effect of the Laser Processing Parameters for Superhydrophilic Fabrication.. .....	17
3.3. Droplet Microarray Design .....	22
3.4. Array Formation .....	24
3.5. Durability and Stability of the Superhydrophobic Surface.....	26
3.6. Durability of the Droplet Microarray .....	27
3.7. Potential Disposable Applications .....	28

3.8. Arbitrary and Complex Patterning .....	30
3.9. Applications as Functional Materials .....	31
CHAPTER 4_SURFACE CHARACTERIZATION_.....	33
4.1. XRD Analysis.....	33
4.2. FT-IR Analysis .....	34
4.3. SEM Analysis.....	36
4.4. EDS Analysis .....	38
4.5. Confocal Microscopic Analysis .....	41
CHAPTER 5_CONCLUSION.....	43
REFERENCES: .....	45

# ACKNOWLEDGEMENT

I would like to express my deepest gratitude to my advisor, Professor Doo-Man Chun, for his great support, and guidance and for providing me with an excellent atmosphere for doing research. I am a novice in conducting research. I can learn how to conduct research from him with his constant supervision. It is a great understatement to say that this work would not have been accomplished without his help. I thank him for his excellent effort and patience with me to train me.

My sincere thanks to my colleagues in the Hybrid Manufacturing Technology laboratory, especially Mr. Malik, who supported me a lot from the beginning of my journey. The outstanding friendly nature inside the laboratory helps me incredibly to do research.

Best regards,

Mohammad Imran Bappy

July 2024

Ulsan, Republic of Korea



# ABSTRACT

Surface wettability is an important phenomenon that has implications in many different scientific domains. It is determined by the interaction between liquids and solid substrates. This study investigates the production of superhydrophobic/superhydrophilic surfaces on aluminum alloy (Al 6061) by non-hazardous chemical treatments and nanosecond-pulse laser processing as an environmentally acceptable method of producing microdroplet arrays. The method used is discontinuous dewetting, which allows for accurate droplet generation without the need for costly automation. Process parameters are optimized to achieve effective water separation between superhydrophilic patterns, and the impact of laser power on water spreading is demonstrated. Surface chemistry and morphology are characterized at each stage of the fabrication process through various analyses. The fabricated surfaces exhibit reliable stability under long exposure to air, freshwater, and intense heat conditions. Additionally, the prospective of using disposable aluminum dishes to produce customizable superhydrophobic surfaces with superhydrophilic arrays is introduced. This eco-friendly approach addresses the need for higher array density platforms with small droplet volumes, particularly relevant for biomedical and pharmacological applications demanding high detection sensitivity and throughput processing.

## **Keywords:**

Superhydrophobic surface; Superhydrophilic patterns; Wettability; Laser texturing; Droplet microarray; precision.

# LIST OF TABLES

Table 1: Fabrication parameters of the laser texturing .....	14
Table 2: Time (s) needed for the 1 $\mu$ L droplet to spread over $2 \times 2$ cm <sup>2</sup> size superhydrophilic surface for each sample and the Laser areal fluence ( $F_a$ , J/mm <sup>2</sup> ). .....	18
Table 3: Variations in the chemical composition of Al 6061 with sample 7 parameters after different stages of surface modification (percentage by weight)..	39
Table 4: Variations in the O/Al, Si/Al superhydrophilic surfaces of different samples with laser areal fluence. ....	40

# LIST OF FIGURES

Figure 1: The number of total published papers each year since 2000 with the “surface wettability” keyword in Web of Science .....	1
Figure 2: Schematic diagram of (a) a superhydrophobic surface, (b) a hydrophobic surface, (c) a hydrophilic surface and (d) a superhydrophilic surface.....	3
Figure 3: Droplet Microarray .....	4
Figure 4: Applications of Droplet Microarray .....	5

Figure 5: Schematic diagram of the laser texturing system and beam path design...	9
Figure 6: Surface modification process for superhydrophobic surface and superhydrophilic patterns.....	10
Figure 7: Laser texturing time for 1 cm <sup>2</sup> area with different laser speeds.....	13
Figure 8: Water droplet's contact angles and sliding angles of the superhydrophobic surfaces fabricated with different laser scanning speeds. ....	17
Figure 9: The spreading stage of 1 μL water droplet at 0, 2, 4 and 6 seconds on the superhydrophilic surface treated with 0.48W laser power during the second laser texturing and fabricated by laser speeds of (a) 250 mm/s, (b) 750 mm/s and (c) 1250 mm/s.....	18
Figure 10: Precision of the wettability over the superhydrophilic round-shaped patterns of 1 mm diameter fabricated with 15 different laser parameters. ....	21
Figure 11: Precision of the wettability over the superhydrophilic square-shaped patterns of 1 mm diameter fabricated with 15 different laser parameters. ....	21
Figure 12: Measuring the error in wettability precision for (a) a round-shaped pattern with a diameter of 1 mm and (b) a square-shaped pattern with a side length of 1 mm. ....	23
Figure 13: The design of the precise droplet microarray.....	24
Figure 14: Formation of droplet arrays on the droplet microarray.....	25

Figure 15: Arrays of water droplets on the precisely designed DMA with superhydrophilic spots of 300 $\mu\text{m}$ diameter .....	26
Figure 16: Durability and stability of superhydrophobic Al 6061 surface after 24 hours at 200°C, after 24 hours under fresh water and after 3 months of storage in ambient air.....	27
Figure 17: Superhydrophobic and superhydrophilic surface fabrication on disposable aluminium dish.....	29
Figure 18: Water repellency of superhydrophobic aluminum foil.....	29
Figure 19: Disposable Droplet Microarray (DMA).....	30
Figure 20: Arbitrary and complex patterning. ....	31
Figure 21: Illustration of (a) bouncing effect of superhydrophobic Al 6061, (b) self-cleaning process of superhydrophobic Al 6061 .....	32
Figure 22: XRD results of the DMA at different stages of the fabrication process.	33
Figure 23: FR-IR results of the DMA at different stages of the fabrication process .....	34
Figure 24: SEM images of the designed DMA at different stages of the fabrication process.....	37
Figure 25: Confocal microscopic images of (a) bare Al 6061 surface, (b) after 1st laser texturing, (c) after boiling water treatment, (d) after silicon oil heat treatment, (e) after 2nd laser texturing and (f) after hot water treatment at 60°C. ....	42

# LIST OF ABBREVIATIONS

Serial No	Short Form	Full Form
1	DMA	Droplet Microarray
2	Al	Aluminum
3	CA	Contact Angle
4	SA	Sliding Angle
5	XRD	X-Ray Diffraction
6	SEM	Scanning Electron Microscope
7	EDS	Energy Dispersive X-ray Spectroscopy
8	FT-IR	Fourier Transform Infrared Spectroscopy

# CHAPTER 1

## INTRODUCTION

### 1.1 Introduction to Surface Wettability

The wettability of solid surfaces has emerged as a vital area of research across various scientific disciplines, spanning from physics and chemistry to materials science and engineering. The wettability phenomenon governs liquids' spreading behaviour on solid substrates and is critical in determining surface energy, adhesion, and contact angle dynamics. Micro and nano-structured surfaces, inspired by nature and exhibiting extreme wettability characteristics have earned considerable attention in various fields including energy, water management, biological sciences, and everyday tasks. The findings from searching the keyword "surface wettability" on the Web of Science demonstrate a continuous increase in published papers since 2000 (See Figure 1).

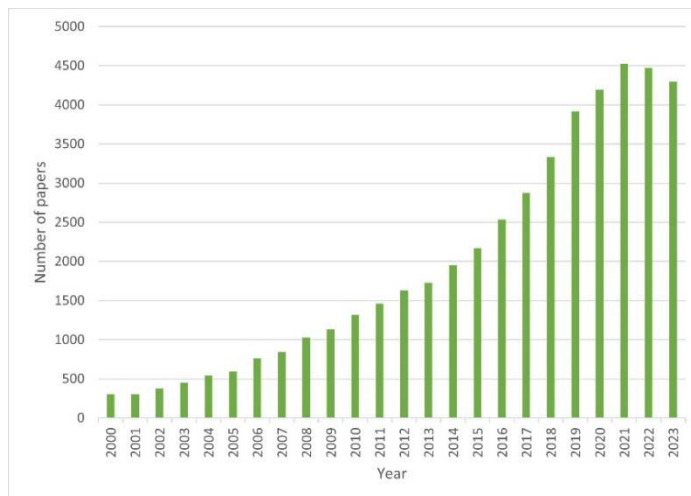


Figure 1: The number of total published papers each year since 2000 with the “surface wettability” keyword in Web of Science

The wetting characteristics of a solid surface are explained using the widely recognized Young, Wenzel and Cassie-Baxter equations [1, 2]. Based on the wettability characteristics, there are four types of solid surfaces: (1) superhydrophobic surfaces, having a contact angle over  $150^\circ$ , (2) hydrophobic surfaces, having a contact angle between  $90^\circ$  and  $150^\circ$ , (3) hydrophilic surfaces, having a contact angle in between  $10^\circ$  and  $90^\circ$ , and (4) superhydrophilic surfaces, having a contact angle below  $10^\circ$  (see Figure 2). The wettability of material surfaces is influenced by two properties. The first property is surface morphology, which contains the structure and roughness of the surface. Generally, if a surface is rougher, it will have a larger contact angle when in contact with a surface of low surface energy. Well-organised and rough surfaces increase the contact angle by reducing the fraction of solid-to-air. The second property is surface chemistry. When two materials come into contact, they typically have a specific surface energy. Surfaces with low surface energy exhibit hydrophobic properties, while those with high surface energy exhibit hydrophilic properties. A microdroplet array can be easily fabricated with many superhydrophilic/hydrophilic patterns, separated by a superhydrophobic barrier.

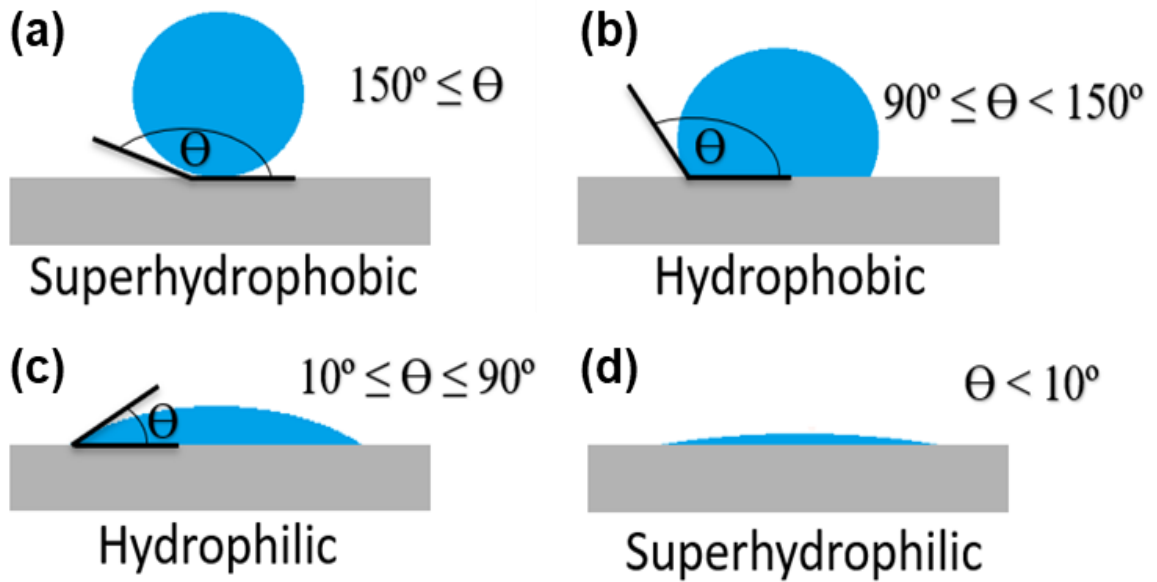


Figure 2: Schematic diagram of (a) a superhydrophobic surface, (b) a hydrophobic surface, (c) a hydrophilic surface and (d) a superhydrophilic surface.

## 1.2 Droplet Microarray

A microdroplet array is a structured arrangement of tiny droplets on a surface, typically at the microscale level. These droplets are usually uniform in size and spacing, and they can be composed of various liquids or solutions depending on the application. This system enables the controllable and precise formation of multiple microsphere droplets of various shapes, sizes, and arrangements [3]. These arrays have a wide range of applications, including wetting behaviour [4-11], thermodynamics [12-14], high-throughput screening [15-22], analysis of cells and tissues [23-27], cell culture [28-30], gel pressure sensor [31], digital PCR [32, 33], DNA synthesis [34] as well as diverse applications for isolating chemical reactions [35], photonics [36], and super-resolution microscopy [37]. As the demand for droplet microarray is increasing for its high detection sensitivity and great



throughput processing, especially in biomedical and pharmacology applications, the need for achieving higher array density platform with small volumes of droplets is on the rise. Furthermore, surface droplets with customizable volumes offer exclusive microenvironments for restricted interfacial reactions and the creation of nanomaterials [38-40].

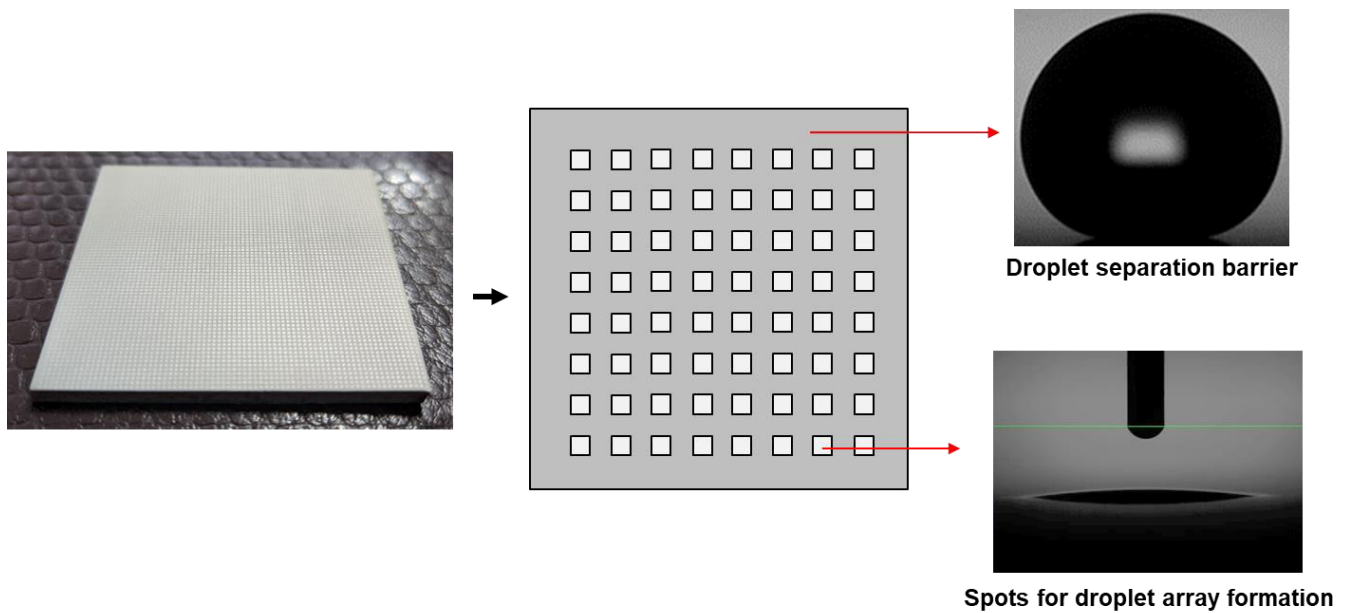


Figure 3: Droplet Microarray

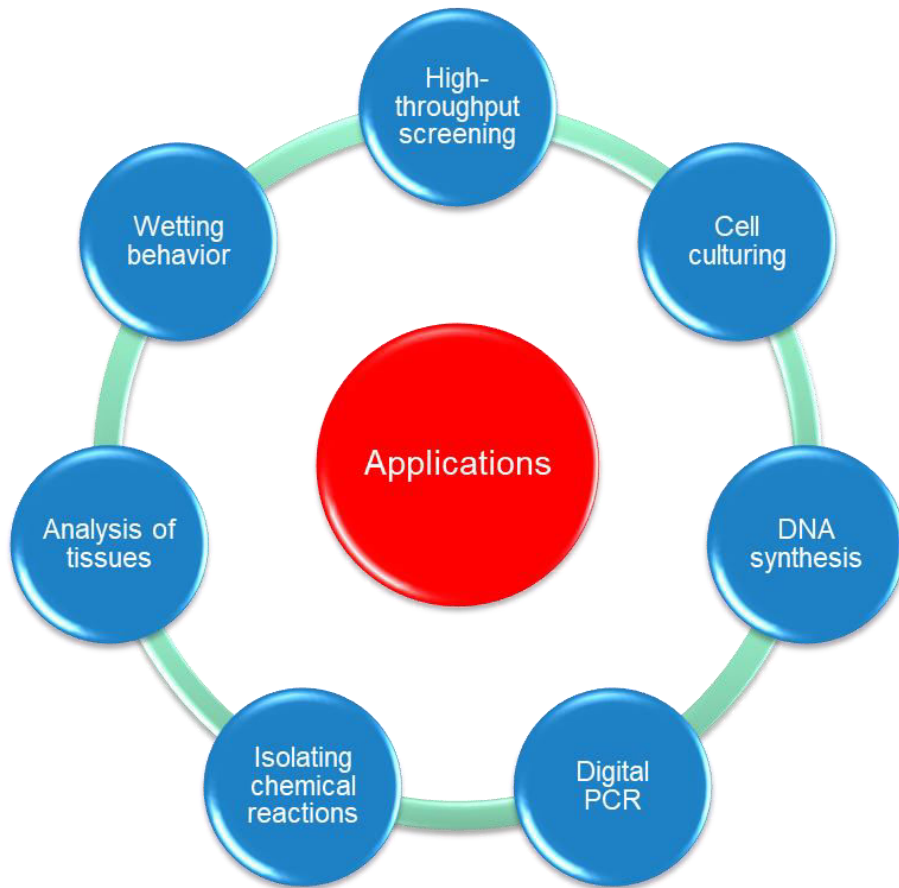


Figure 4: Applications of Droplet Microarray

### 1.3 Previous Trends in Droplet Microarray Research

In recent years, researchers have developed many sophisticated methods to create efficient DMA networks including the wet etching technique [22], inkjet printing [13, 15-17, 26, 28, 29], microfluidics [3, 20, 41], laser fabrication [42], dropping droplets using microscale cavities [43], and more. Most current research focuses on producing complex droplets and employs methods that are mainly suitable for demonstrating the rapid formation of droplet arrays [44, 45]. Although progress in the fabrication of microdroplet arrays has been substantial, a major drawback in

many of these studies is the reliance on toxic chemicals [3, 19]. According to M. Awashra, the approaches to the partition of droplets with controlled volume can be categorized into three sections: generation droplets using a microfluidic pump, confining droplets in a solid container and open microarray system of placing droplets onto a flat surface using a printing technique or discontinuous dewetting [46]. Discontinuous dewetting is an effective technique that facilitates the creation of numerous microdroplets in an open-air system with precise shapes, sizes, and predetermined positions on a structured surface [43, 47, 48]. One of the benefits of this method is that it does not rely on expensive robotics or automation, making it appealing for tasks like diagnostics, cell screening, or medical applications. In the discontinuous dewetting process, fluid is directed across a surface with pronounced dewettability, featuring areas highly prone to wetting, to form an array.

#### **1.4 Objectives of Our Research**

In our study, we propose an eco-friendly method to create a microdroplet array by creating superhydrophobic/superhydrophilic surfaces on aluminum alloy using a nanosecond-pulse laser machine, followed by non-hazardous chemical procedures. A range of process parameters was investigated to determine the optimal conditions for achieving effective water separation between the superhydrophilic patterns. The impact of laser power on the spreading of water on the superhydrophilic spots was also demonstrated. In addition, the surface morphology and chemistry were examined at each stage of fabrication using a series of surface analyses. The fabricated superhydrophobic and superhydrophilic surfaces demonstrate good stability, even when exposed to prolonged periods of air, freshwater, and high-temperature environments. Furthermore, we introduce the potential of using

disposable aluminum dishes to produce superhydrophobic surfaces featuring customizable superhydrophilic arrays.

The objectives of our research are as follows:

1. Sustainable manufacturing of the DMA with no complicated chemical process.
2. Selective patterning of DMA.
3. Study the wettability precision of the superhydrophilic patterns.
4. Increase the array density of the DMA.
5. Introduce the potential of disposable applications.
6. Demonstrate additional applications as functional materials.

# CHAPTER 2

## EXPERIMENT

### 2.1 Materials

In this research, Al 6061 sheets with a purity of 95.8-98.6% (obtained from The Nilaco Corporation, Japan) were employed. The samples had dimensions of 40mm×40mm×2mm. Ultrasonic cleaning was performed for 10 minutes using Isopropyl Alcohol with a purity of 99.5% (supplied by the Daejung Chemicals Company Ltd., Republic of Korea). In addition, a silicon oil heat treatment process was conducted using KF96 silicon oil with a viscosity of 100cs (obtained from the Shin-Etsu Chemical Company Ltd., Japan).

### 2.2 Laser Texturing System

Figure 5 displays the direct connection between a high-speed laser scanning system (Model: G07-355-10-B-Red; supplied by the Beijing JCZ Technology Company Ltd) and a Q-switched Nd: YAG nanosecond pulsed ultraviolet (UV) laser source (Model: Grace X 355-12; supplied by the Suzhou Inngu Laser Company, Ltd.). Computer software controlled the 355 nm wavelength pulse laser with an 18 ns pulse duration, which followed the design patterns through the scanning system. The Z-axis stage system allowed easy adjustment of the distance from the scanner lens to the sample surface, enabling precise focusing of the laser beam on the top surface. At the focusing point, a beam diameter of 40  $\mu\text{m}$  was achieved. Two types of overlap factors: lateral and transverse overlap are frequently employed to manage the surface's shape and structure [49, 50]. The chosen approach for creating the pattern, as demonstrated in Figure 5, involved using a line-by-line design with a step size

corresponding to the transverse overlap distance. The lateral overlap distance is controlled by the pulse-to-pulse distance. It was accomplished by varying the laser speed while keeping the pulse frequency fixed at 50000 Hz. To attain a surface with uniform wetting properties in all directions, it is necessary for the transverse overlap distance and the lateral overlap distance to be identical. To determine the power of the laser beam emitted from the galvohead and to texture the metal surface, a laser power meter (A-30-D25-HPB, Laserpoint, Italy) was employed for measurement.

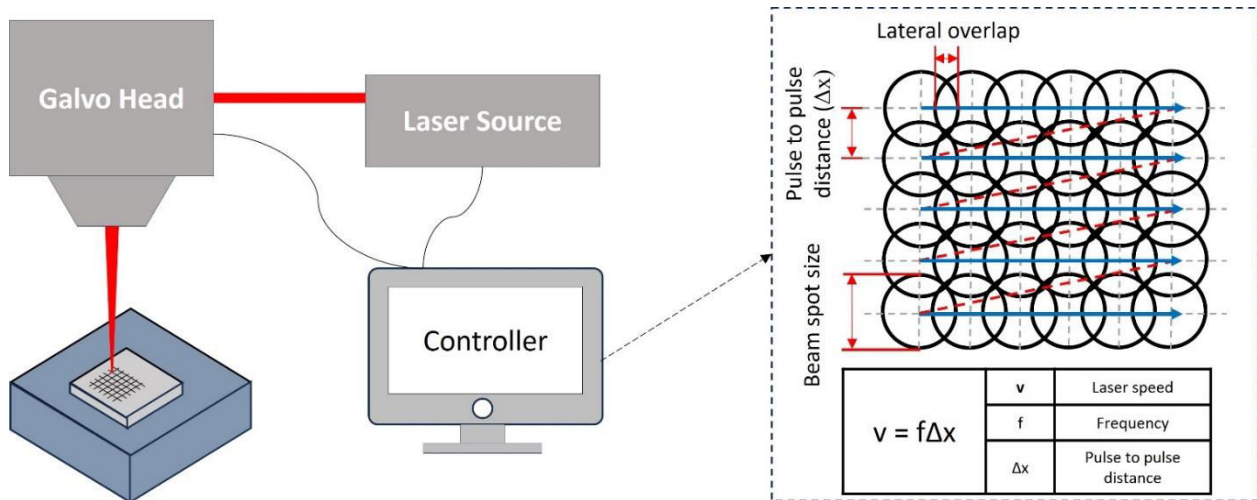


Figure 5: Schematic diagram of the laser texturing system and beam path design.

### 2.3 Fabrication Process

The fabrication process comprises two stages: creating the superhydrophobic surface initially, followed by the formation of superhydrophilic patterns on the background of this surface, as illustrated in Figure 6.

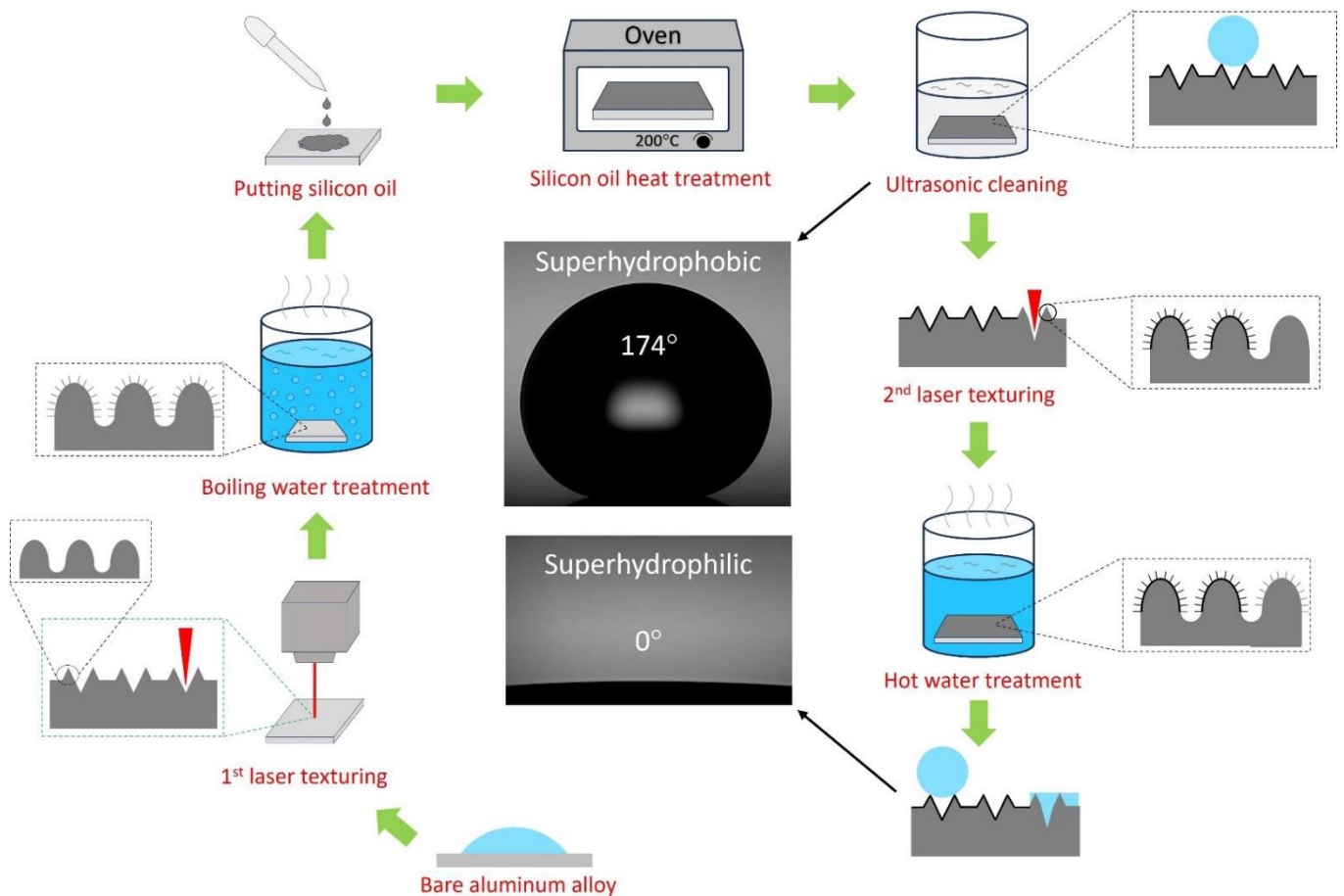


Figure 6: Surface modification process for superhydrophobic surface and superhydrophilic patterns.

To fabricate the superhydrophobic surface, the aluminum alloy was textured by the laser machine to create microstructure and enhance the surface roughness. Subsequently, the sample was subjected to boiling water immersion for 10 minutes, which facilitated the development of nanostructures on the surface. Following this, the roughened surface was completely covered with the silicon oil and put inside a conventional oven at 200°C for 1 hour. Through this process, the surface absorbed organic superhydrophobic compounds from the surrounding air, thereby achieving a low energy state. Any remaining silicon oil was eliminated by cleaning the sample with isopropyl alcohol in an ultrasonic cleaner. The ultrasonic cleaning procedure was conducted twice for 5 minutes each. At this point of the fabrication process, the sample transformed into a superhydrophobic surface.

To generate the superhydrophilic patterns on the previously prepared superhydrophobic surface, laser texturing was selectively performed, resulting in the surface becoming hydrophilic. Following this, the sample was submerged in hot water at 60°C for 10 minutes, resulting in the formation of enduring superhydrophilic patterns. The wettability of the initially created superhydrophobic surface remained unchanged during the subsequent hot water treatment. It has been reported that superhydrophobic fabrication should always be done first as the superhydrophilic surface can transform into a superhydrophobic surface when the silicon oil heat treatment is executed [51].

For all the samples, the surface texturing was done only one time. The laser speed and the step size were the same for both 1st and 2nd laser texturing for every sample. The laser texturing control unit enabled adjustment of laser power as a percentage. The fabrication involved selecting percentages of 40%, 65%, and 90%, with corresponding average laser powers of 0.48W, 1.3W, and 3W, as measured by the



laser power meter. The laser power remained consistent throughout the fabrication process to create the superhydrophobic surface. Conversely, when fabricating the superhydrophilic surface, three distinct laser powers were employed for each laser speed and its corresponding step size. Figure 7 shows the laser texturing time needed for a 1 cm<sup>2</sup> area by five different laser speeds. The laser areal fluence (F<sub>a</sub>) was estimated utilizing the following equation [52].

$$F_a = N \frac{P}{v \times \Delta x}$$

Where P (W) is the laser beam power, N is the number of repetitions of the laser texturing on the surface, v (mm/s) is the speed of the laser scanning beam, and Δx (mm) is the step size. As the laser texturing was done one time for each sample, the value of N is 1.

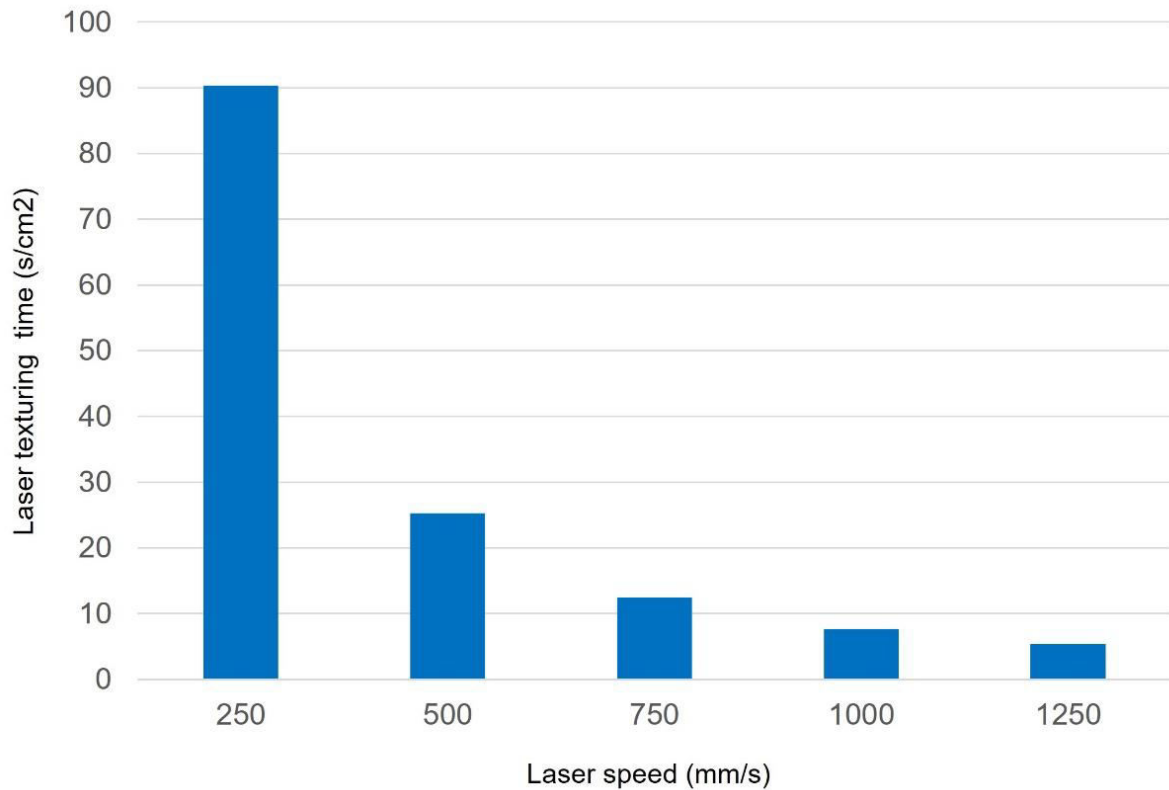


Figure 7: Laser texturing time for 1 cm<sup>2</sup> area with different laser speeds.

The laser texturing parameters are specified in Table 1. For the parameter study, five different laser speeds were used. All samples intended for superhydrophobic fabrication were textured with a laser power of 3W. For superhydrophilic patterns, three different laser powers were applied during the second laser texturing for each laser speed. Consequently, a total number of 15 samples were fabricated and subjected to further investigation.

**Table 1: Fabrication parameters of the laser texturing**

Sample	Laser speed v (mm/s)	Step size $\Delta x$ ( $\mu\text{m}$ )	Lateral overlap percentage (%)	Laser power (W)		Laser areal fluence $F_a$ ( $\text{J}/\text{mm}^2$ )	
				1 <sup>st</sup> laser texturing	2 <sup>nd</sup> laser texturing	1 <sup>st</sup> laser texturing	2 <sup>nd</sup> laser texturing
1	250	5	87.5	3	0.48	2.56	0.384
2	250	5	87.5	3	1.3	2.56	1.04
3	250	5	87.5	3	3	2.56	2.4
4	500	10	75	3	0.48	0.64	0.096
5	500	10	75	3	1.3	0.64	0.26
6	500	10	75	3	3	0.64	0.6
7	750	15	62.5	3	0.48	0.284	0.0426
8	750	15	62.5	3	1.3	0.284	0.115
9	750	15	62.5	3	3	0.284	0.266
10	1000	20	50	3	0.48	0.16	0.024
11	1000	20	50	3	1.3	0.16	0.065
12	1000	20	50	3	3	0.16	0.15
13	1250	25	37.5	3	0.48	0.1024	0.0153
14	1250	25	37.5	3	1.3	0.1024	0.0416
15	1250	25	37.5	3	3	0.1024	0.096

## 2.4 Material Characterization

The wetting and dewetting characteristics of the modified surfaces were assessed using a measuring device of contact angle (SmartDrop, supplied by the Femtofab Company Ltd., Korea). The morphology of the surface for different samples was analyzed using field-emission scanning electron microscopy (FE-SEM, JSM-6500 F; JEOL, Japan). Also, a range of surface analyses were carried out to reckon the induced changeover in the surface chemistry at each stage of the fabrication process for a selective sample. These analyses included energy dispersive X-ray spectroscopy (EDS, JSM-6500-F, JEOL, Japan), Fourier transform infrared spectroscopy (FT-IR, Varian 670-IR; VARIAN, USA), and X-ray diffraction spectroscopy (XRD, Ultima IV; RIGAKU, Japan) in the range from  $10^\circ$  to  $90^\circ$ . Moreover, a laser-operated confocal microscope (VK-X200 series; supplied by the Keyence Corporation, Japan) was used to obtain three-dimensional (3D) surface topography pictures, which resulted in the measuring of the surface roughness.

# CHAPTER 3

## RESULTS AND DISCUSSION

### 3.1 Effect of the Laser Processing Parameters for Superhydrophobic Fabrication

It has been reported that the altering of laser scanning speed [53] and the step size [54] during laser texturing have a significant impact on the wetting properties of a solid surface. So, to examine the wetting characteristics of the superhydrophobic surfaces, the contact angle (CA) and the sliding angle (SA) of water were measured with water droplets of  $10 \pm 1 \mu\text{L}$  volume. Figure 8 shows the average value of contact angles and sliding angles measured at five different positions of each sample. The error bars indicate the maximum and the minimum values in both cases. The figure indicates all the samples have contact angles higher than  $150^\circ$  and sliding angles lower than  $10^\circ$ .

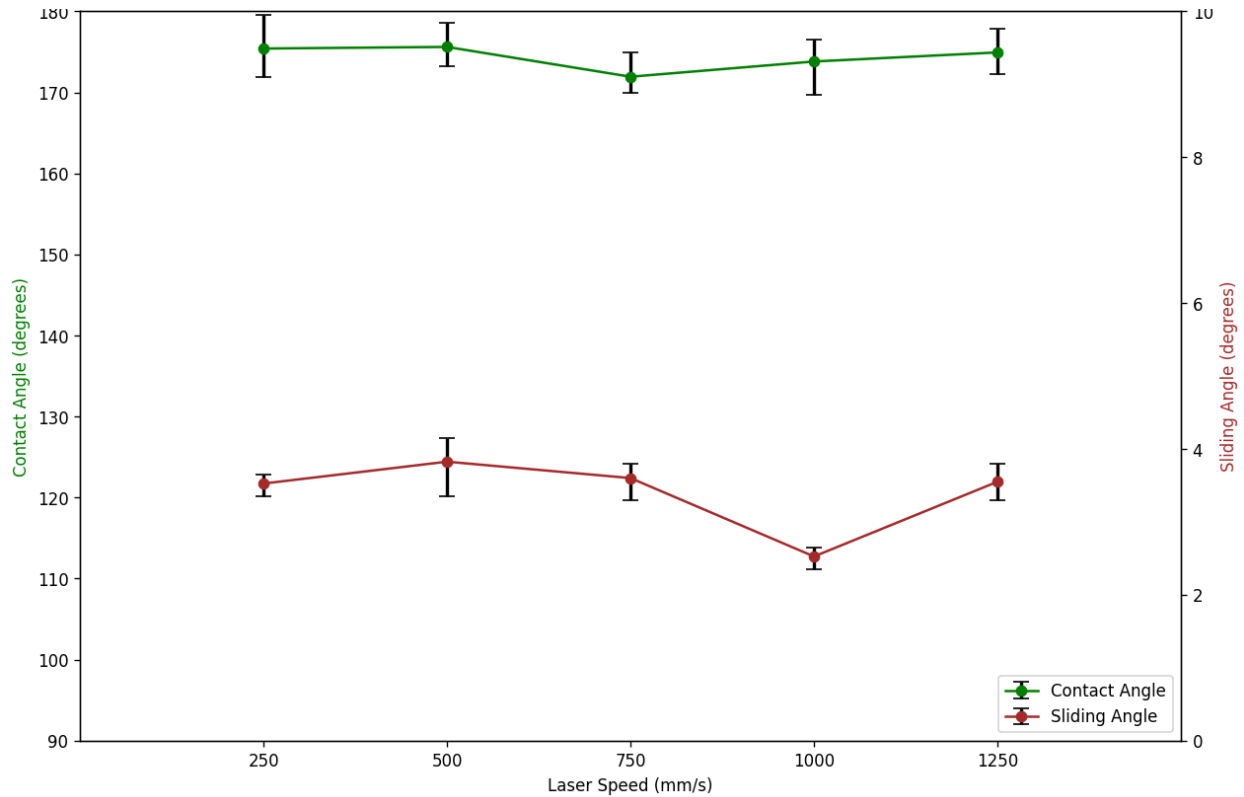


Figure 8: Water droplet's contact angles and sliding angles of the superhydrophobic surfaces fabricated with different laser scanning speeds.

### 3.2 Effect of the Laser Processing Parameters for Superhydrophilic Fabrication

After going through all the steps of the fabrication process, the aluminum alloy substrates become superhydrophilic ( $CA < 10^\circ$ ) with all the fabrication process parameters, except the shaded sample parameter in Table 2. An alternative method other than measuring contact angles was used to evaluate the superhydrophilic surfaces' performance. Using the contact angle meter device, which was previously mentioned, a water droplet of  $1 \mu\text{L}$  was touched with the superhydrophilic surface of  $2 \times 2 \text{ cm}^2$  of each sample, as shown in Figure 9. The time for the water droplet to spread until becoming completely horizontal with the surface was measured and shown in Table 2.

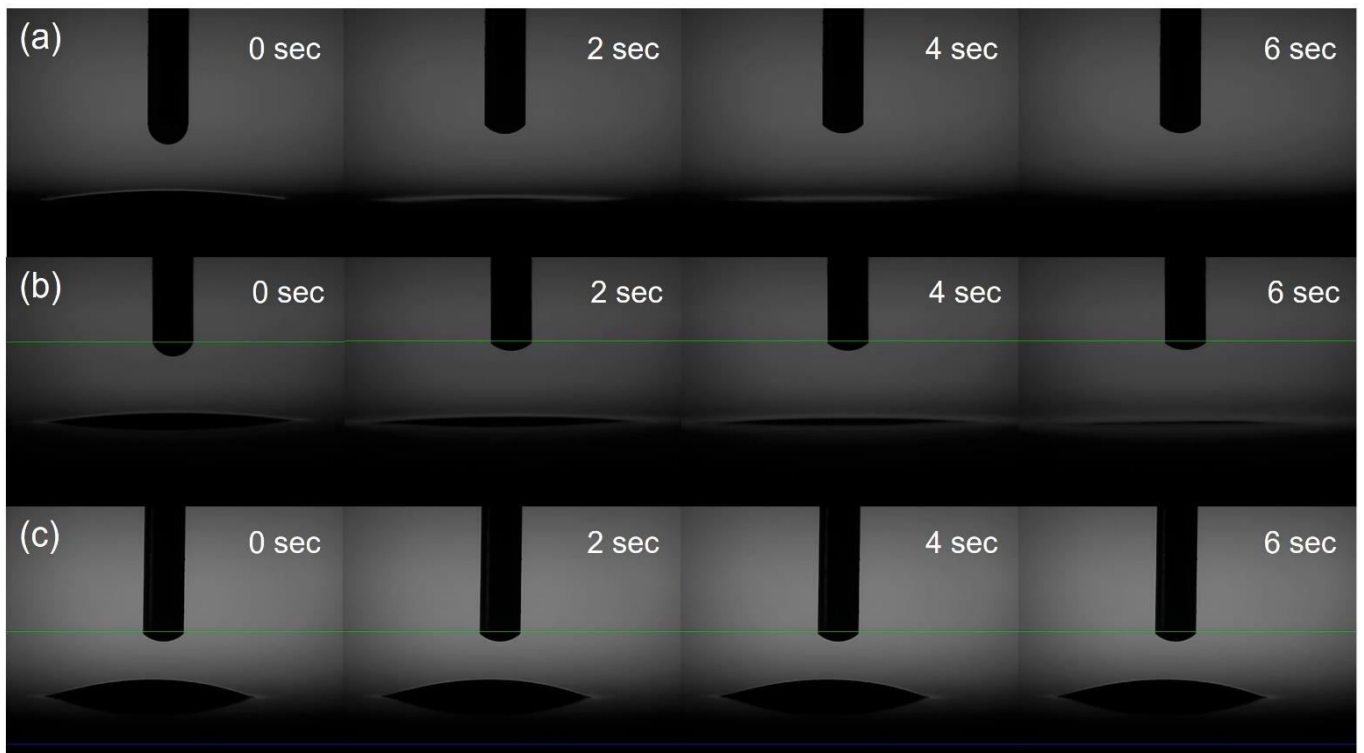


Figure 9: The spreading stage of 1  $\mu\text{L}$  water droplet at 0, 2, 4 and 6 seconds on the superhydrophilic surface treated with 0.48W laser power during the second laser texturing and fabricated by laser speeds of (a) 250 mm/s, (b) 750 mm/s and (c) 1250 mm/s.

**Table 2: Time (s) needed for the 1  $\mu\text{L}$  droplet to spread over  $2 \times 2 \text{ cm}^2$  size superhydrophilic surface for each sample and the Laser areal fluence ( $F_a$ ,  $\text{J}/\text{mm}^2$ ).**

Laser speed \ Laser power	250	500	750	1000	1250
	(mm/s)	(mm/s)	(mm/s)	(mm/s)	(mm/s)
0.48 W	t = 3.25	t = 3.78	t = 4.73	No spreading	No spreading
	$F_a = 0.384$	$F_a = 0.096$	$F_a = 0.0426$	$F_a = 0.024$	$F_a = 0.0153$
1.3 W	t = 2.43	t = 2.65	t = 3.16	t = 3.38	No spreading
	$F_a = 1.04$	$F_a = 0.26$	$F_a = 0.115$	$F_a = 0.065$	$F_a = 0.0416$
3 W	T = 1.94	t = 2.41	t = 2.87	t = 3.08	t = 3.12
	$F_a = 2.4$	$F_a = 0.6$	$F_a = 0.266$	$F_a = 0.15$	$F_a = 0.096$

Table 2 demonstrates that increasing the energy input per unit area leads to improved superhydrophilicity performance. Based on this evaluation, it can also be concluded that aluminum 6061 alloy surfaces cannot achieve superhydrophilicity with a laser areal fluence below 0.0416 J/mm<sup>2</sup>. Figure 9 shows the difference of 1 uL water droplet spreading at 0, 2, 4 and 6 seconds on the superhydrophilic surface for three different samples that were treated with 0.48W of laser power during the second laser texturing and created at laser speeds of 250 mm/s, 750 mm/s, and 1250 mm/s. The lower speed provides a higher laser texturing energy on the surface, resulting in faster spreading of water over the surface. As the increased value laser areal fluence (Fa) influences the superhydrophilic performance, there are two ways to increase the value: (1) decreasing the laser speed and (2) increasing the laser power. By keeping the laser speed constant, the laser power was increased to 1.3W and 3W to make superhydrophilic patterns with higher laser areal fluence. However, high laser power causes a significant impact on the borderline of the patterns and allows some debris to spread over the boundary edge. These spread particles cause an extra region outside the borderline to become superhydrophilic. As a result, droplets can spread outside the borderline of the patterns and hamper the precision of the laser patterning. To evaluate this issue, superhydrophilic patterns round-shaped with a 1 mm diameter and square-shaped with a 1 mm side length for each parameter mentioned in Table 1 were tested to check the precision. To ensure droplet formation of a diameter not exceeding the pattern's length during this experiment, the minimum volume to be dropped on the pattern was calculated by the following equation.

$$V = \frac{\pi h}{6} (3r^2 + h^2)$$

Here, V is the volume, r is the radius, and h is the height of the droplet. The minimum volume for 1 mm diameter patterns was calculated to be 0.261 uL. So, a droplet of



0.2±0.05  $\mu\text{L}$  was dropped on the patterns. After that, images of the patterns were taken by an area scan camera (Basler ace acA2440-75uc, supplied by Basler AG, Germany). Figure 10 and Figure 11 demonstrate the precision of the patterns for each sample (according to Table 1) with round-shaped patterns and square-shaped patterns respectively. The superhydrophilic patterns fabricated with higher laser power show less precision in both figures. The water spreads over the borderline of the patterns due to the previously mentioned reason for the debris spreading outside the pattern's boundary. The direction of the excessive spreading is uncontrollable due to the airflow inside the laser texturing chamber. To ensure precise wettability, the laser power for the 2nd laser texturing should be as low as possible. However, decreasing the laser power below 40% (0.48W) shows some untextured areas among the patterns. As a result, 0.48W was chosen to be the lowest laser power for the fabrication of the superhydrophilic patterns.

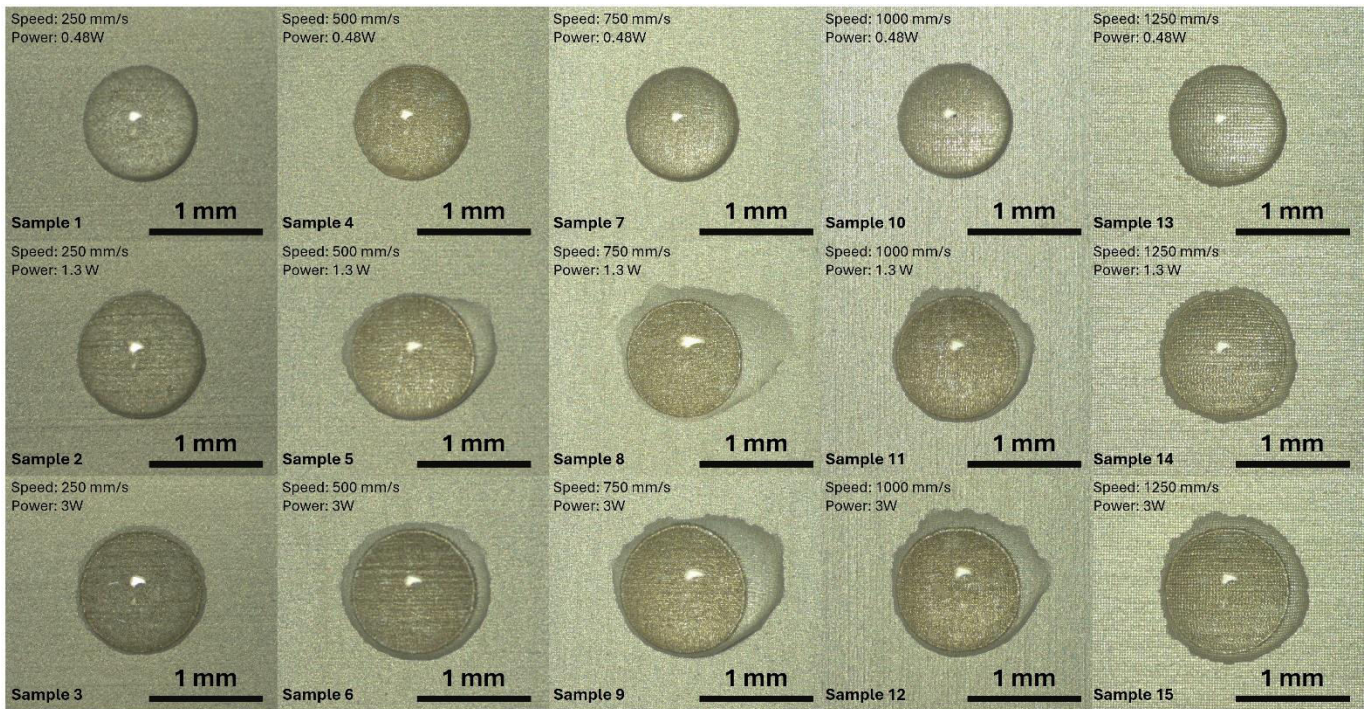


Figure 10: Precision of the wettability over the superhydrophilic round-shaped patterns of 1 mm diameter fabricated with 15 different laser parameters.

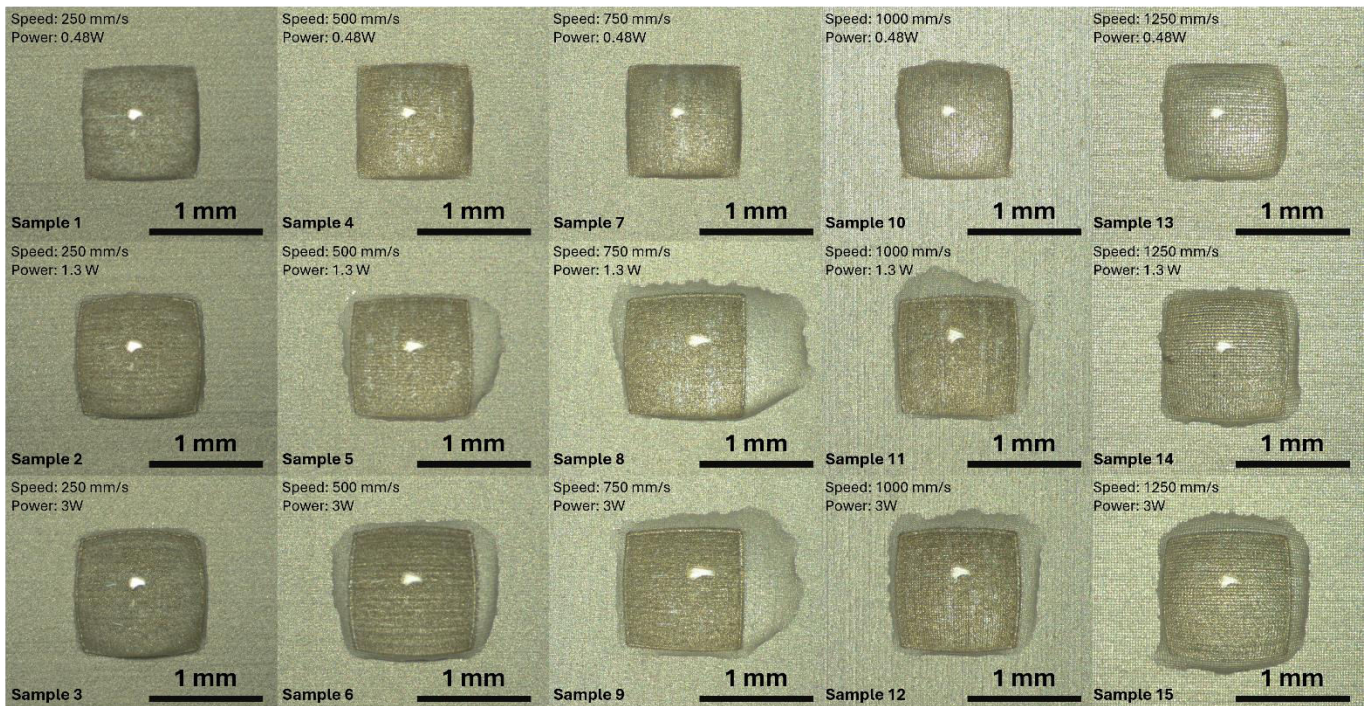


Figure 11: Precision of the wettability over the superhydrophilic square-shaped patterns of 1 mm diameter fabricated with 15 different laser parameters.

### 3.3 Droplet Microarray Design

When designing a Droplet Microarray (DMA), two key factors need to be balanced: fabrication efficiency and array density. Higher laser power during fabrication of the arrays can compromise wettability precision (Figures 10 & 11). According to the measurement of the error in wettability precision shown in Figure 12, samples no 1, 4 and 7 show less than 10% excessive length of wettability. Notably, round-shaped patterns exhibited superior wettability control compared to squares under identical parameters. Also, all three samples show good superhydrophilic performance as discussed in Table 2. Fabrication time is another crucial consideration. Faster processing reduces costs, improves efficiency, and facilitates mass production. Among the qualifying samples, sample 7 exhibited the shortest processing time (Figure 7). Therefore, considering both superhydrophilicity, fabrication time, and the 10% wettability precision threshold, the process parameters used for sample 7 (laser speed 750 mm/s, step size 15  $\mu\text{m}$ , first laser texturing power 3W and second laser texturing power 0.48W) were chosen for the final DMA design.

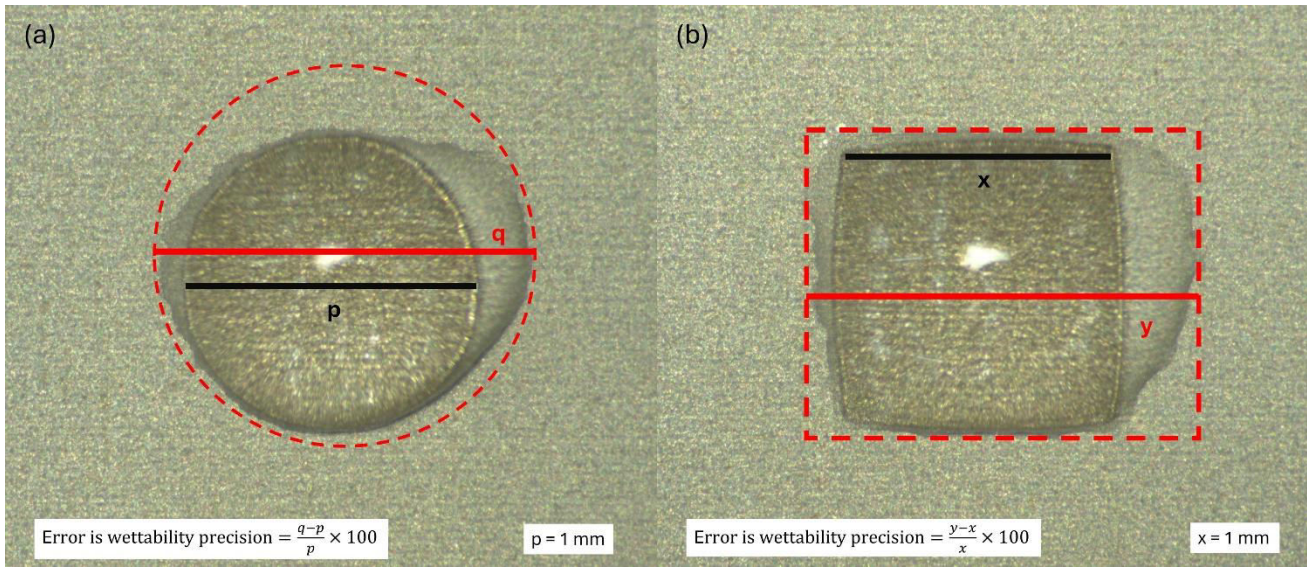


Figure 12: Measuring the error in wettability precision for (a) a round-shaped pattern with a diameter of 1 mm and (b) a square-shaped pattern with a side length of 1 mm.

Levkin et al. introduced a DMA slide design with a square-shaped spot array offering an approximate density of 244 spots/cm<sup>2</sup> [29]. The spots were hydrophilic with a side length of 350 μm and a spacing of 150 μm between each spot. In contrast, our design utilizes a circular spot array with superhydrophilic patterns. Our design achieves a density of approximately 333 spots/cm<sup>2</sup>, with each spot having a diameter of 300 μm and a spacing of 250 μm. This spacing was determined by accounting for a 200 μm wettability precision tolerance for adjacent superhydrophilic patterns and an additional margin of 50 μm. The design and arrangement can be seen in Figure 13..

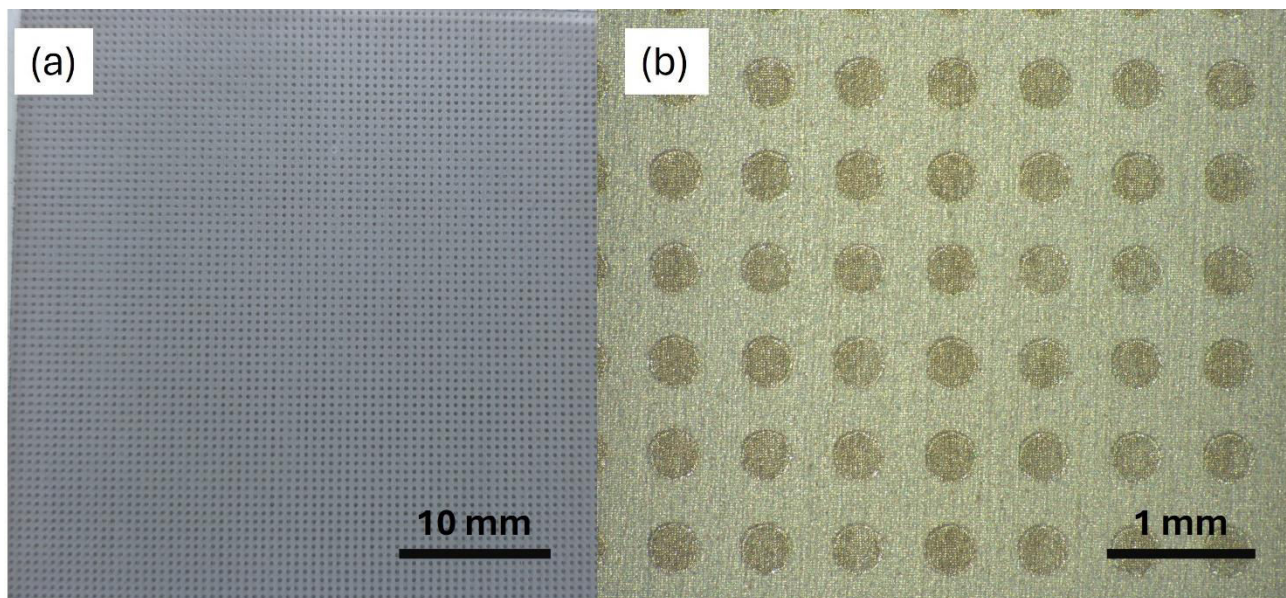


Figure 13: The design of the precise droplet microarray.

### 3.4 Array Formation

To create arrays of droplets, the DMA was immersed in fresh water and then withdrawn. This process resulted in droplets forming on the superhydrophilic spots. The precise design of the DMA includes very small superhydrophilic spots, which are not visible without magnification. To demonstrate the array formation, a DMA was fabricated with the same parameters as sample 7, featuring superhydrophilic spots of 2 mm in diameter and spaced 3.5 mm apart centre-to-centre. The array formation is illustrated in Figure 14.

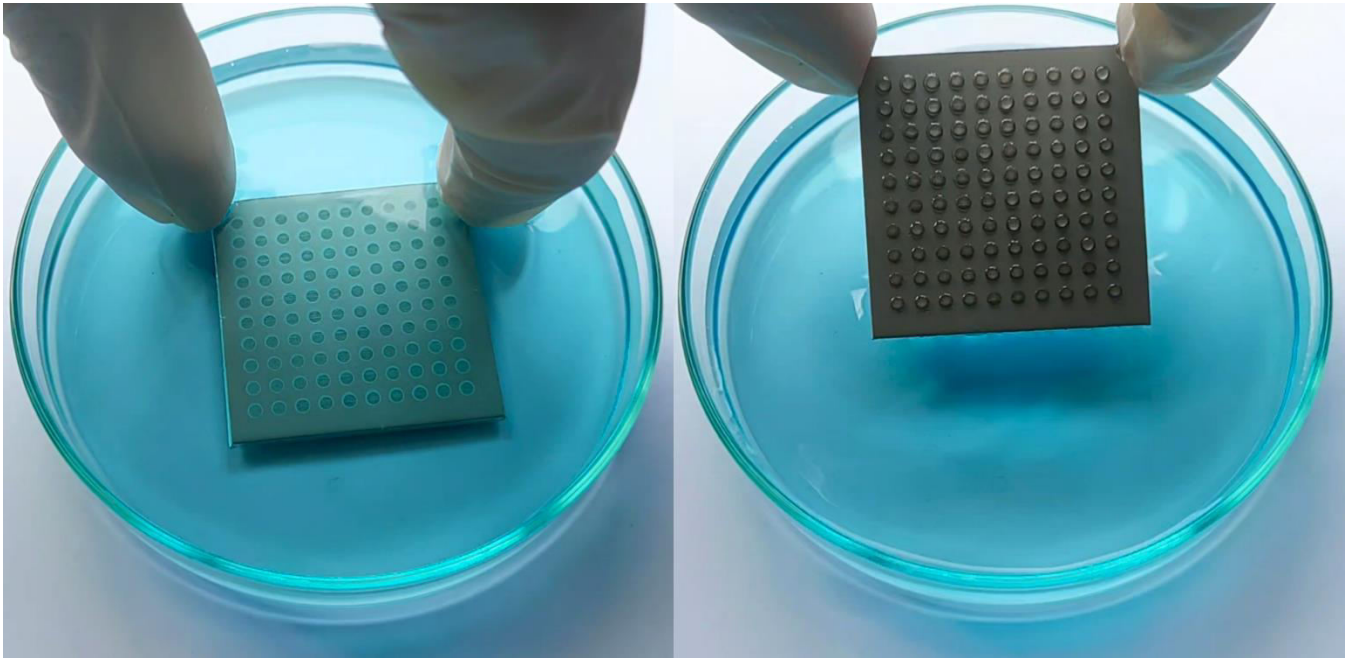


Figure 14: Formation of droplet arrays on the droplet microarray.

By following the similar procedure shown in Figure 14, droplet arrays were formed on the precise DMA. As the water droplets were very small, images were captured with the area scan camera (Baser ace acA2440-75uc, supplied by Basler AG, Germany) and it is shown in Figure 15.

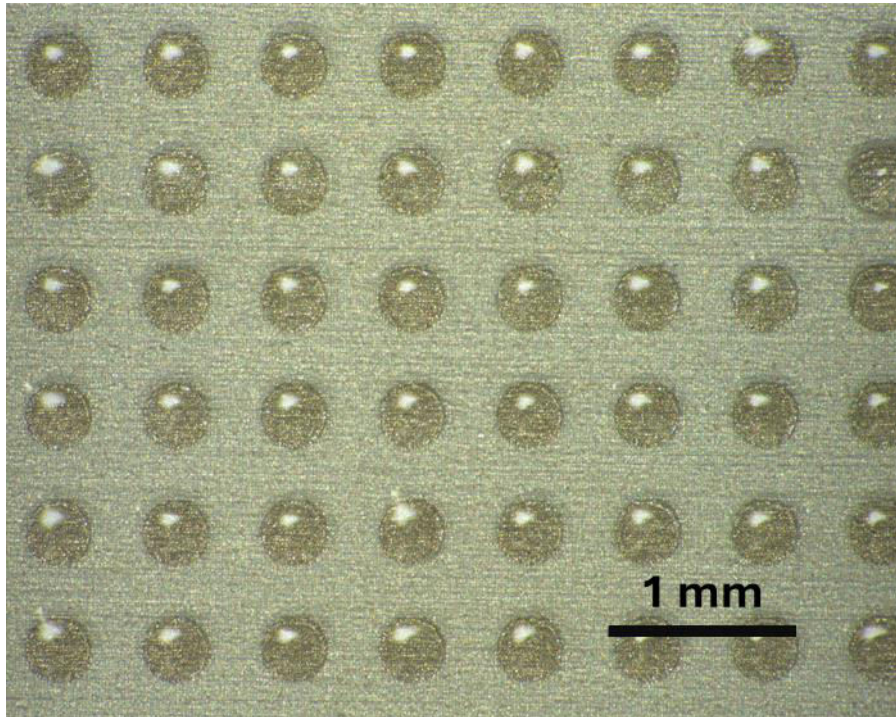


Figure 15: Arrays of water droplets on the precisely designed DMA with superhydrophilic spots of 300  $\mu\text{m}$  diameter.

### 3.5 Durability and Stability of the Superhydrophobic Surface

The durability and stability of a functional material are crucial because it ensures consistent performance over time, preventing degradation or failure that could compromise its intended function. It also contributes to the reliability, longevity, and cost-effectiveness of applications utilizing the material. To assess the durability and stability of the fabricated Al 6061 superhydrophobic surface (before the 2nd laser texturing), separate samples (prepared using parameters of sample 7) were subjected to various conditions: oven exposure (200°C, 24 hours), immersion in freshwater (24 hours), and ambient air storage (3 months). After each treatment, contact angle and sliding angle measurements were taken at five different positions on the sample. Figure 16 displays the average contact and sliding angles. The results indicate that

the fabricated sample maintained contact angles greater than  $150^\circ$  and sliding angles less than  $10^\circ$  after all treatments, demonstrating excellent durability and stability.

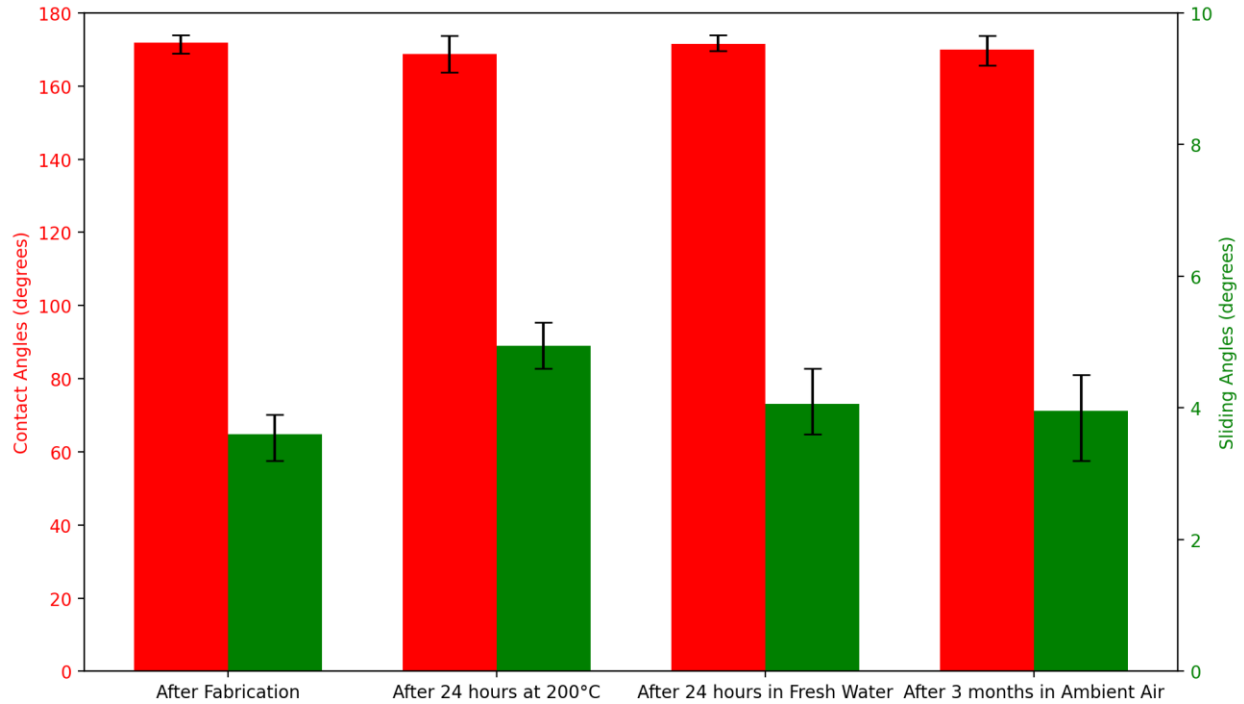


Figure 16: Durability and stability of superhydrophobic Al 6061 surface after 24 hours at  $200^\circ\text{C}$ , after 24 hours under fresh water and after 3 months of storage in ambient air

### 3.6 Durability of the Droplet Microarray

As previously mentioned, one of the major applications of a DMA slide is cell culturing. Contamination with microorganisms or chemicals in cell culturing can lead to erroneous and irreproducible results and autoclaving is the most reliable and effective method to prevent such outcomes. Autoclaving is a sterilization technique that is done for 60-90 min at  $121^\circ\text{C}$ . The designed DMA with superhydrophilic spots of 2 mm diameter was placed in an oven at  $121^\circ\text{C}$  for 90 minutes. Before oven treatment, droplet arrays were formed on the DMA by immersing it in fresh water, with an average droplet volume of  $0.9724 \mu\text{L}$  per superhydrophilic spot. After the



oven treatment, the process was repeated, resulting in an average droplet volume of 0.9303  $\mu\text{L}$ . Additionally, the superhydrophilic patterns retained good water adhesion after heat exposure, indicating that the designed DMA is suitable for the autoclaving process.

### **3.7 Potential Disposable Applications**

Disposable materials play a crucial role in modern society by offering convenience, efficiency, and often cost-effectiveness in various applications. Their ability to fulfil specific functions temporarily or for a single use reduces maintenance requirements and enhances hygiene standards. Moreover, they contribute to sustainable practices by minimizing the need for extensive cleaning processes and conserving resources. To assess the feasibility of implementing the proposed manufacturing technique for creating disposable superhydrophobic and superhydrophilic surfaces, fabrication experiments were conducted on a Disposable Aluminum Dish (SL. Dis8051, provided by SciLab Korea, Republic of Korea). Figure 17 demonstrates the superhydrophobic surface and superhydrophilic arrays, fabricated on disposable aluminum dish.



Figure 17: Superhydrophobic and superhydrophilic surface fabrication on a disposable aluminium dish.

A superhydrophobic surface was created on aluminium foil further to demonstrate the viability of the proposed fabrication process. The performance of this fabricated superhydrophobic aluminium foil is shown in Figure 18. The results highlight its excellent water repellency, with water droplets forming nearly spherical shapes and easily rolling off the surface.

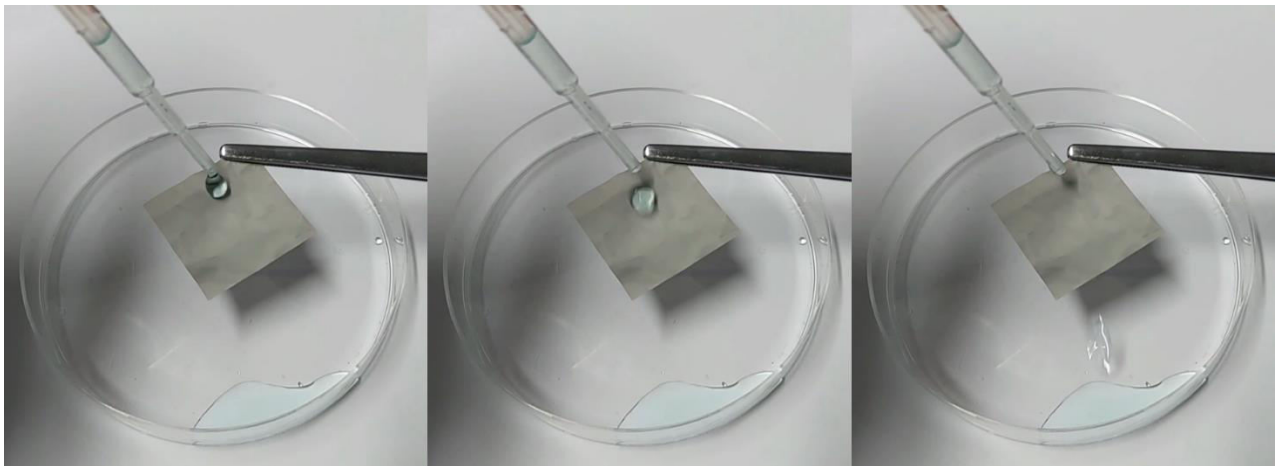


Figure 18: Water repellency of superhydrophobic aluminum foil.

Subsequently, the disposable aluminum foil was further processed to create a disposable droplet microarray (DMA), shown in Figure 19. The disposable DMA combines the flexibility and light weight of aluminum foil with the functionality of advanced microarray technology, making it ideal for high-throughput screening and single-use diagnostic applications.

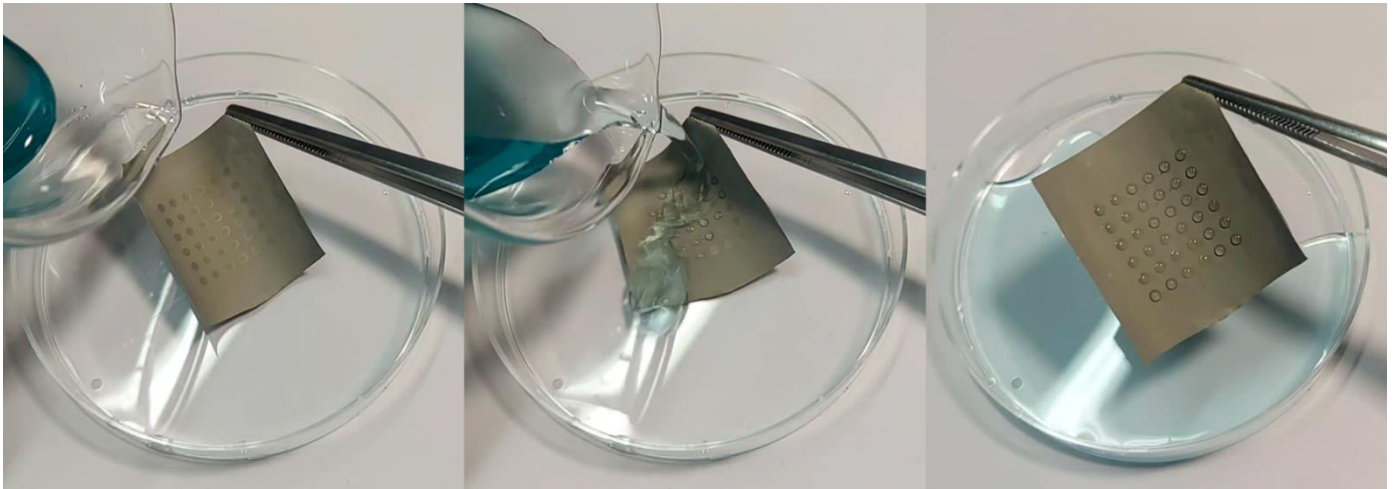


Figure 19: Disposable Droplet Microarray (DMA)

### 3.8 Arbitrary and Complex Patterning

One of the key advantages of the proposed manufacturing process is its ability to create arbitrary and complex patterns without the need for extra masks or additional treatments. Any intricate CAD-designed pattern can be textured onto the superhydrophobic metallic surface and subsequently rendered superhydrophilic through a hot water treatment process. This flexibility allows for the precise customization of surface properties, making it highly adaptable for a wide range of applications, from biomedical devices to microfluidic systems. The ability to easily switch between superhydrophobic and superhydrophilic states also enhances the functionality and versatility of the fabricated surfaces, opening up new possibilities

for innovative designs and applications in various scientific and industrial fields. Figure 20 shows some examples of the complex patterns and arrays.

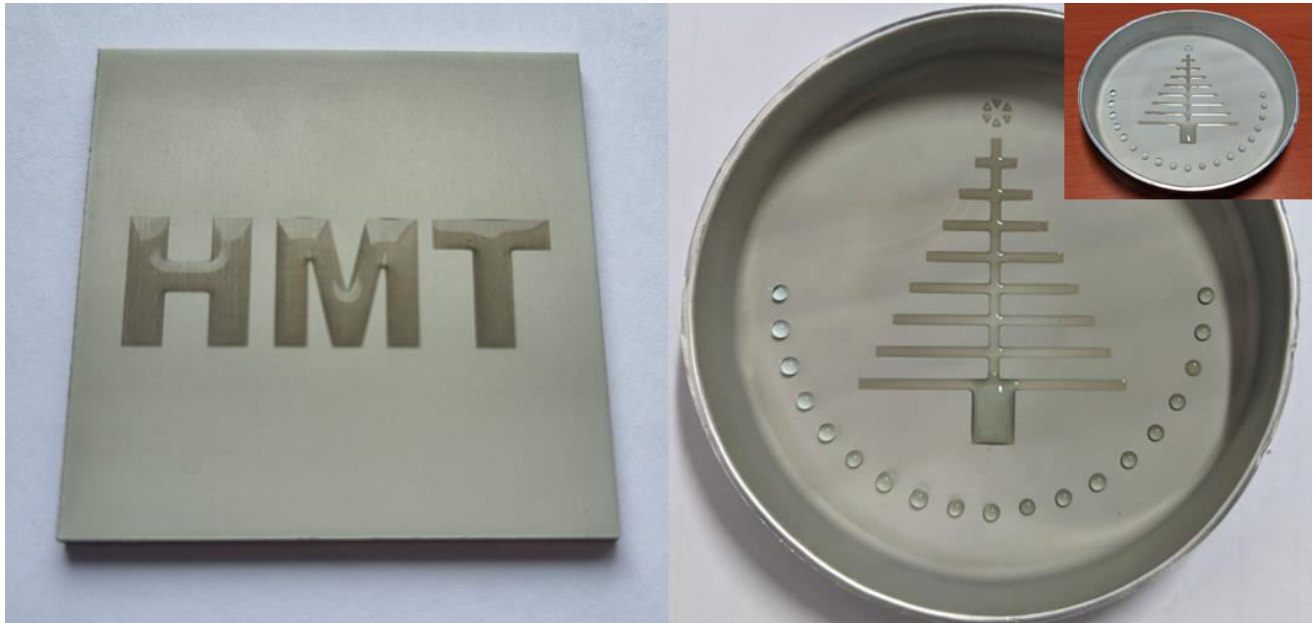


Figure 20: Arbitrary and complex patterning.

### 3.9 Applications as Functional Materials

Functional materials are a class of materials specifically engineered to exhibit unique properties and perform functions beyond merely providing structural support. These materials are designed to interact with their environment and respond to external stimuli such as heat, light, electric or magnetic fields, chemical agents, and mechanical stress in beneficial ways. Functional materials play a crucial role in a wide array of advanced technologies and applications, driving innovation in fields such as electronics, energy, biotechnology, and nanotechnology.

Using our fabricated superhydrophobic surfaces, we have demonstrated (Figure 21) two key applications of these functional materials: (a) the bouncing effect, where

water droplets rebound off the surface due to its extreme water repellency, and (b) the self-cleaning effect, where contaminants are easily removed by water droplets rolling off the surface, maintaining cleanliness without the need for manual intervention. These applications highlight the potential of functional materials to enhance performance, efficiency, and convenience in various practical contexts.

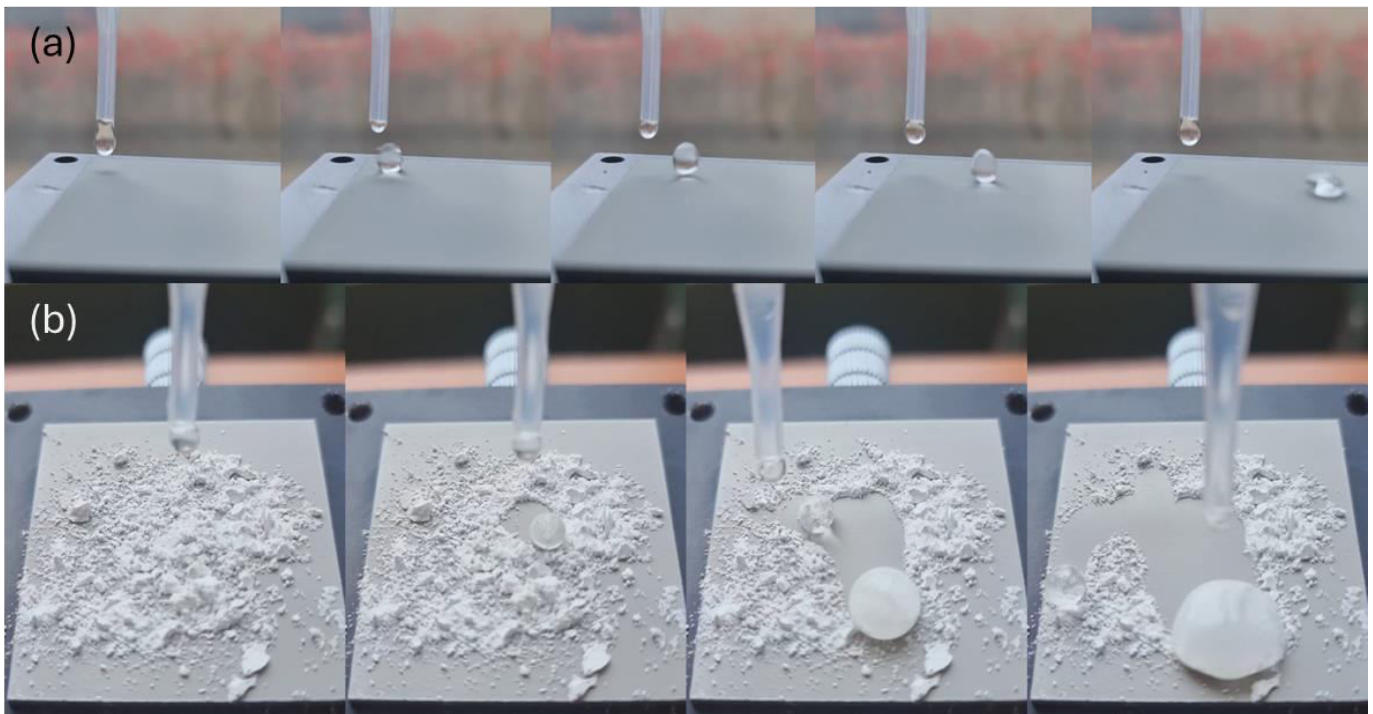


Figure 21: Illustration of (a) bouncing effect of superhydrophobic Al 6061, (b) self-cleaning process of superhydrophobic Al 6061

# CHAPTER 4

## SURFACE CHARACTERIZATION

### 4.1 XRD Analysis

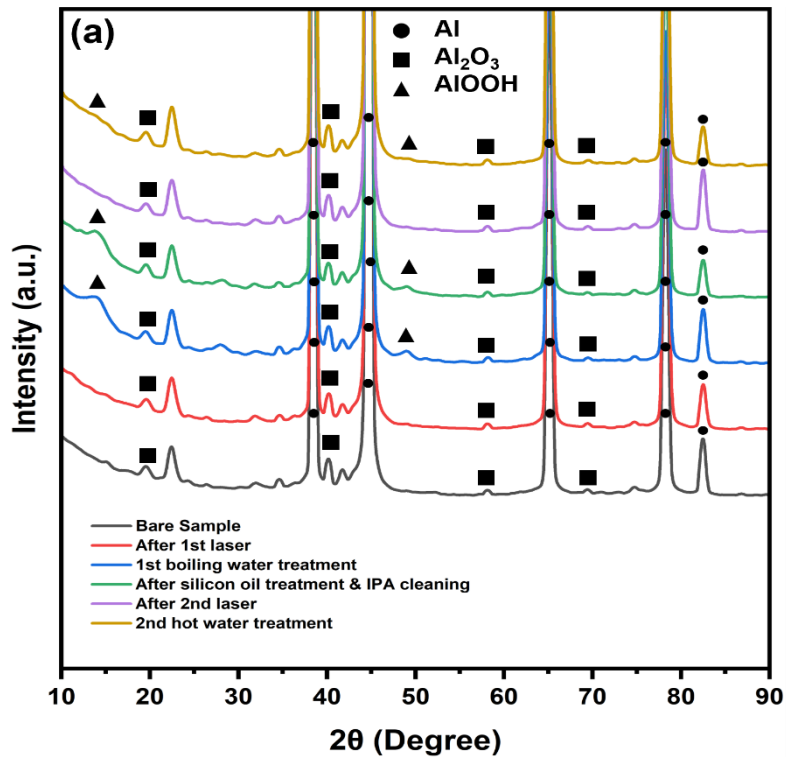


Figure 22: XRD results of the DMA at different stages of the fabrication process.

In the XRD analysis shown in Figure 22, only aluminum and aluminum oxide peaks were visible in both the bare and 1st laser-textured samples. However, after the boiling water treatment, a new peak corresponding to AlOOH, a hydrophilic pseudo-boehmite structure, was confirmed, indicating the formation of a new nanostructure in the sample. This AlOOH peak was also observed after treatments with silicon oil and hot water. Notably, the peak was absent following the 2nd laser texturing, likely due to the increased surface roughness induced by the process [55-57].

## 4.2 FT-IR Analysis

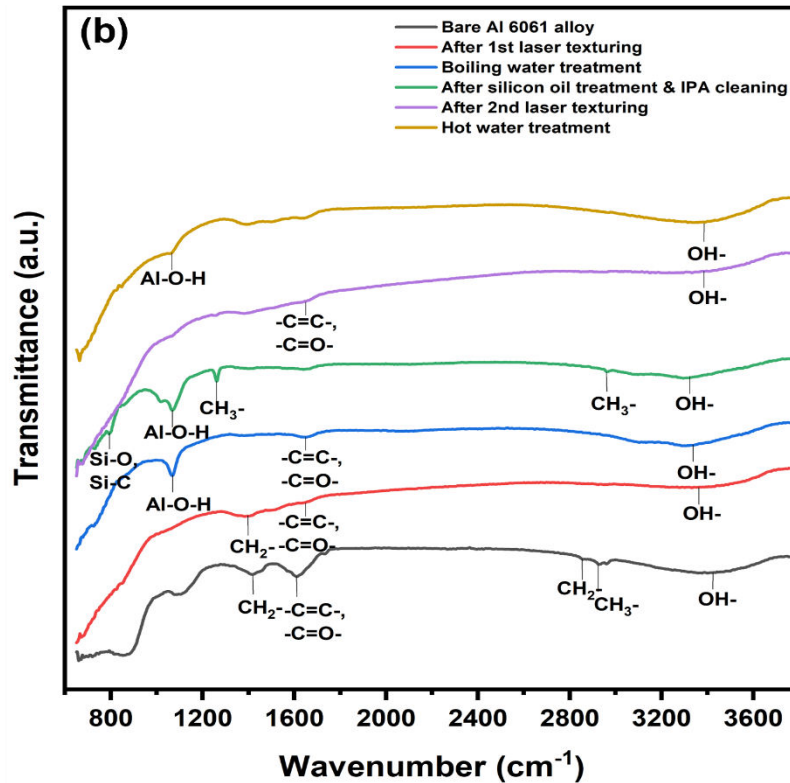


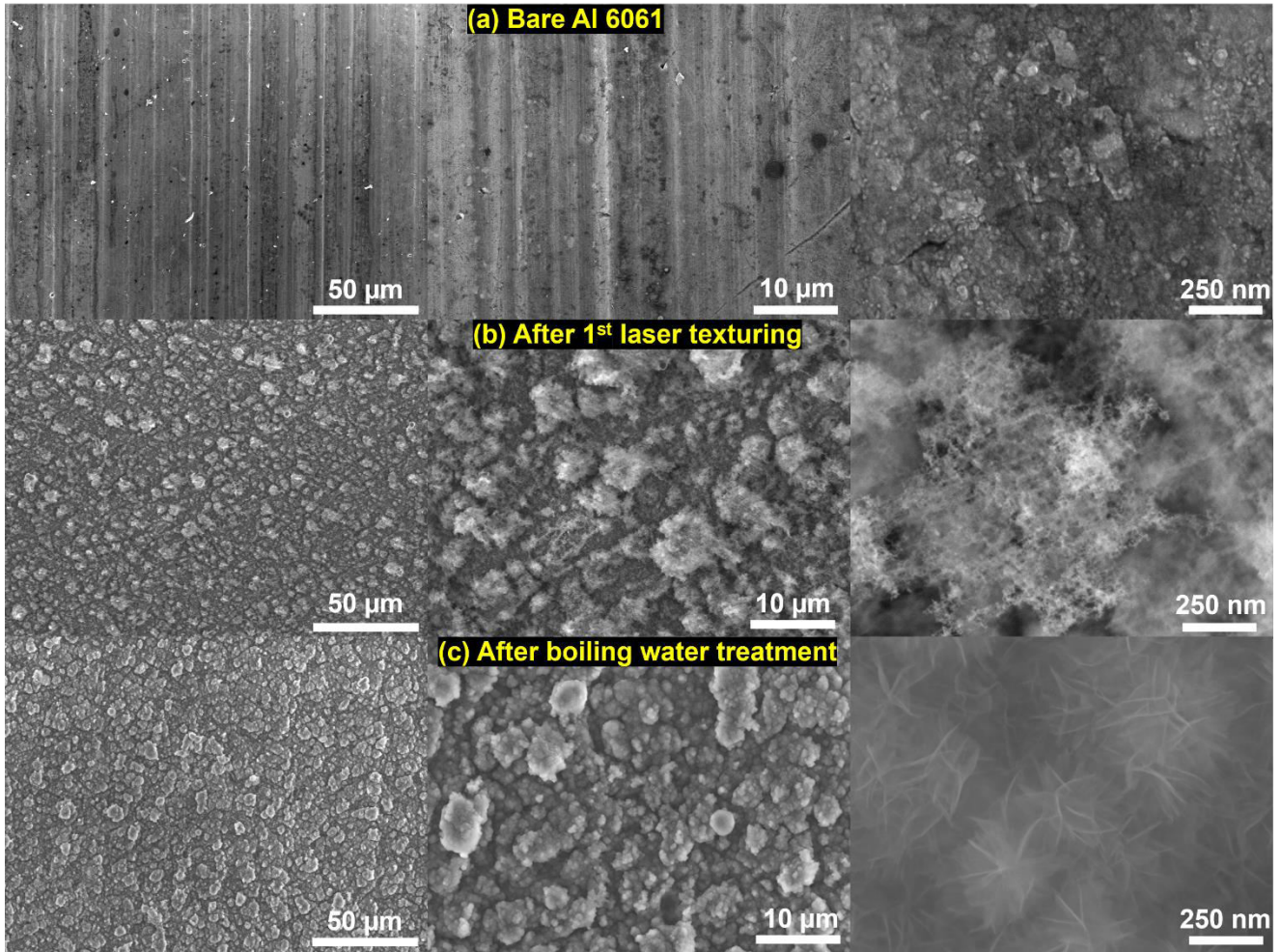
Figure 23: FR-IR results of the DMA at different stages of the fabrication process.

Further insights were gained through FTIR analysis (Figure 23), revealing a distinctive band at  $1064.52\text{ cm}^{-1}$  indicative of the Al-O-OH bond formation post boiling water, silicon oil, and hot water treatments. Notably, the disappearance of CH<sub>2</sub> and CH<sub>3</sub> strong hydrophobic groups at  $2854.15\text{ cm}^{-1}$  and  $2925.5\text{ cm}^{-1}$  respectively, observed in the bare Al 6061 alloy, after the 1st laser texturing underscores the removal of the superhydrophobic surface by the laser. Conversely, following the silicon oil treatment, new bands associated with Si-O/Si-C and CH<sub>3</sub> emerged at  $794.5\text{ cm}^{-1}$ ,  $1259.3\text{ cm}^{-1}$ , and  $2960.22\text{ cm}^{-1}$ , reflecting the introduction of hydrophobic components onto the surface. This transformation was further corroborated by the significant increase in weight percentage observed in EDS analysis post-silicon oil treatment, confirming the development of a superhydrophobic surface.

### 4.3 SEM Analysis

Figure 24 presents Scanning Electron Microscopy (SEM) images at three magnifications, illustrating the micro and nanoscale features of sample 7. The bare Al 6061 surface is initially smooth; however, distinct micro and nanostructures emerge after the first laser texturing, as depicted in Figure 24(b). No significant morphological changes were observed at the microscale following boiling water and silicon oil treatments. Nonetheless, the formation of entirely new nanostructures is evident at the nanoscale. These novel structures, resulting from the interaction between aluminium and boiling water, resulted as hydrophilic pseudo-boehmite structures, supported by XRD and FTIR analyses [60, 61]. In second laser texturing, the microstructures resemble those formed after the first texturing, but with decreased microstructures in their number. The hydrophilic pseudo-boehmite structures reappear following the hot water treatment but with a small size because of the temperature being lower at 60°C, indicating that surface morphology is influenced by both the laser parameters and the subsequent hot water treatment.





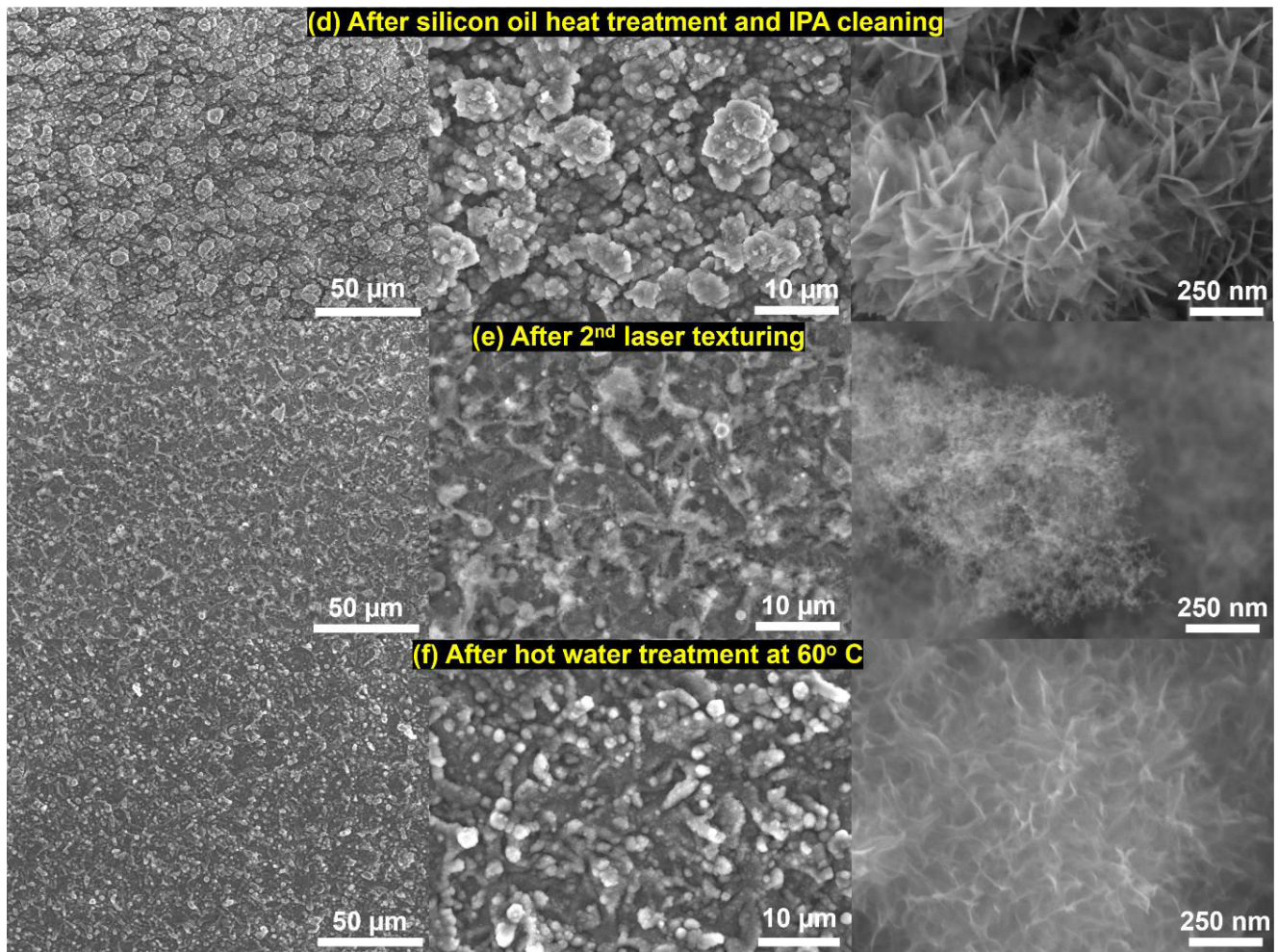


Figure 24: SEM images of the designed DMA at different stages of the fabrication process.

#### 4.4 EDS Analysis

Based on the EDS results presented in Table 3, the increased weight ratio between oxygen and aluminum (O/Al) further confirms the formation of the pseudo-boehmite structure by the boiling water heat treatment. This observation is corroborated by FTIR analysis, which shows a prominent band at  $1064.52\text{ cm}^{-1}$ , indicating the presence of Al-O-OH bonds following the boiling water, silicon oil, and hot water treatments. After the 2<sup>nd</sup> laser texturing, the nanostructures were destroyed. After the hot water treatment at  $60^{\circ}\text{C}$ , the nanostructures were formed again. However, the ratio of (O/Al) was less compared to the boiling water heat treatment process. This concludes higher temperature of the water enhances the formation of the nanostructure. These complementary analyses collectively validate the structural transformation and confirm the successful formation of hydrophilic pseudo-boehmite on the treated surfaces. In addition, the increased weight ratio of (C/Al) after the silicon oil heat treatment confirms the organic absorption of the  $\text{CH}_3$  compound from the air by the metallic substrate, making the sample superhydrophobic.

**Table 3: Variations in the chemical composition of Al 6061 with sample 7 parameters after different stages of surface modification (percentage by weight)**

Elements	Bare Al 6061	After 1 <sup>st</sup> laser texturing	After boiling water treatment	After silicon heat treatment & IPA cleaning	After 2 <sup>nd</sup> laser texturing	After hot water treatment at 60°C
Al	87.60	76.33	31.49	26.0	78.21	51.73
O	7.41	21.80	67.67	60.28	17.41	47.37
Si	0.82	0.19	0.21	4.08	0.57	0.17
C	0.45	0.23	0	9.33	1.73	0
Mg	3.12	1.12	0.50	0.10	1.29	0.41
Fe	0.60	0.33	0.12	0.21	0.80	0.31
O/Al	0.084	0.286	2.149	2.318	0.223	0.916
C/Al	0.005	0.003	0	0.359	0.022	0
Si/Al	0.009	0.002	0.007	0.157	0.007	0.003

Further analysis of the surface morphology was conducted on the surfaces of various samples (samples 1, 3, 8, 9, 13, 15) to assess the impact of varying laser areal fluence ( $F_a$ ) for confirming super hydrophilicity behaviour under specific parameters and compared the results with sample 7. With EDS results, we observed that with increasing energy input (Laser areal fluence), an increased O/Al weight ratio was observed and faster water droplets spreading whereas, the Si/Al ratio remained almost the same, as shown in the table. Notably, sample 13, characterized by the second lowest energy input, exhibits microscale grids as shown in Figure, having Si/Al ratio higher than other samples showing no spreading time suggesting, it can be hydrophilic or hydrophobic.

**Table 4: Variations in the O/Al, Si/Al superhydrophilic surfaces of different samples with laser areal fluence.**

Sample	Spreading time (s)	Laser areal fluence $F_a$ (J/mm <sup>2</sup> )	O/Al	Si/Al
Sample 3	1.94	2.4	2.32	0.003
Sample 1	3.25	0.384	2.03	0.003
Sample 9	2.87	0.266	2.06	0.001
Sample 8	3.16	0.115	2.02	0.005
Sample 15	3.12	0.096	1.41	0.006
Sample 7	4.73	0.0426	0.916	0.003
Sample 13	No spreading	0.0153	1.13	0.025

#### 4.5 Confocal Microscopic Analysis

The average surface roughness of the Al 6061 alloy at each stage of the surface treatment was also analyzed by the laser scanning confocal microscope, shown in Figure 25. Significant increases in surface roughness (Sa) were observed after the 1st laser texturing and the boiling water heat treatment, supporting the formation of microstructures and nanostructures from the FE-SEM images in Figure 24. The roughness decreased after the 2<sup>nd</sup> laser texturing as it destroyed the previously created micro and nanostructures. The roughness again increases after hot water treatment due to newly formed nanostructures. Thus, the roughness of the surface at each stage of the fabrication process alligns with the outcomes of the FEM-SEM and XRD analysis.

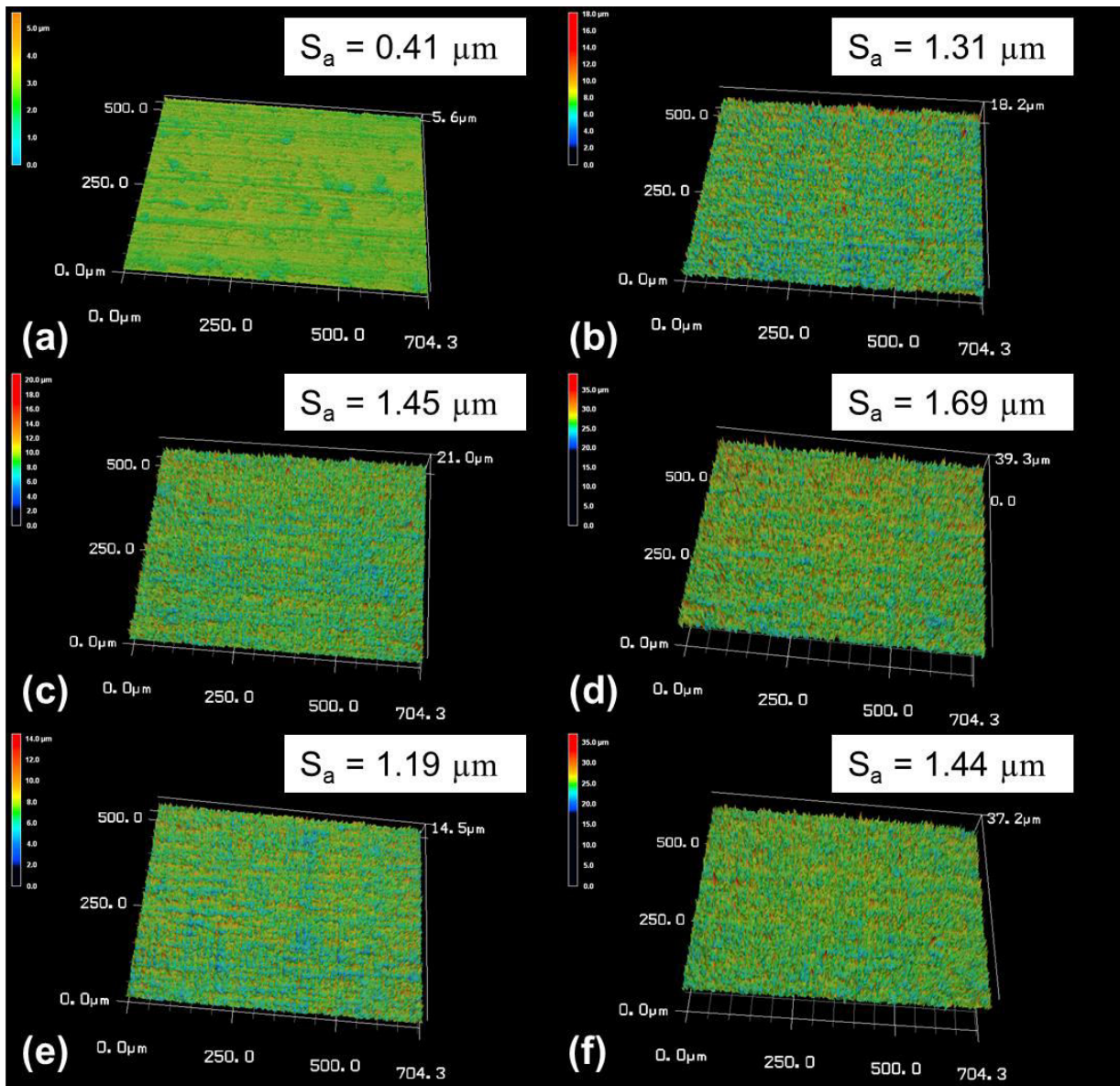


Figure 25: Confocal microscopic images of (a) bare Al 6061 surface, (b) after 1st laser texturing, (c) after boiling water treatment, (d) after silicon oil heat treatment, (e) after 2nd laser texturing and (f) after hot water treatment at  $60^\circ\text{C}$ .

# CHAPTER 5

## CONCLUSION

An eco-friendly method to fabricate superhydrophobic/superhydrophilic surfaces on aluminum alloy 6061 was demonstrated using non-hazardous chemical treatments and nanosecond-pulse laser processing. Process parameters such as laser speed, step size, and power were optimized to achieve effective water separation between superhydrophilic patterns with good spreading characteristics. The nano-micro hierarchical composite architectures were attained through the combination of laser texturing for creating microstructures and the generation of pseudo-boehmite nanostructures by boiling water heat treatment. Surface morphology and chemistry analyses confirmed the presence of hydrophilic pseudo-boehmite nanostructures and low surface energy compounds responsible for the superhydrophobic and superhydrophilic wetting behaviours. The wettability characteristics of the superhydrophobic and superhydrophilic surfaces for each sample were investigated by the measurement of contact angle, sliding angle, and spreading of water droplets. The effect of laser parameters on the superhydrophilic surface fabrication was evaluated and wettability precision was established. By analyzing the wettability precision, the optimum laser parameters were chosen to design a droplet microarray with a density of 333 spots/cm<sup>2</sup>. The fabricated surfaces exhibited excellent stability and durability, withstanding prolonged exposure to air, fresh water, high temperatures, scratching, and autoclaving conditions suitable for cell culture applications. The versatility of the proposed method was demonstrated by creating



arbitrary superhydrophilic patterns on disposable aluminum dishes, enabling open-air droplet transportation for potential applications. The eco-friendly nature, high precision, good stability, and ability to pattern disposable substrates make this fabrication approach promising for various applications requiring controlled wettability. Future work could explore scaling up the process for industrial manufacturing and integrating the patterned surfaces into functional devices across different fields.

# REFERENCES

1. Chu, W.-S., et al., Green Fabrication of Superhydrophobic Surfaces Using Laser Surface Texturing Without Toxic Chemicals: A Review. *International Journal of Precision Engineering and Manufacturing*, 2024: p. 1-23.
2. Masduzzaman, M. and B. Kim, Effects of dissimilar molecular interface and ion-concentration on wetting characteristics of nanodroplets. *Microfluidics and Nanofluidics*, 2021. 25: p. 1-14.
3. Guo, X., et al., Droplet Microfluidic-Based Low-Cost and High-Speed Microsphere Array Direct Writing Technology and Its Applications. *ACS Applied Materials & Interfaces*, 2023. 15(26): p. 32047-32056.
4. Eslami, F. and J.A. Elliott, Stability analysis of microdrops during concentrating processes. *The Journal of Physical Chemistry B*, 2014. 118(13): p. 3630-3641.
5. Gennes, P.-G., F. Brochard-Wyart, and D. Quéré, *Capillarity and wetting phenomena: drops, bubbles, pearls, waves*. 2004: Springer.
6. Lohse, D. and X. Zhang, Surface nanobubbles and nanodroplets. *Reviews of modern physics*, 2015. 87(3): p. 981.
7. Méndez-Vilas, A., A.B. Jódar-Reyes, and M.L. González-Martín, Ultrasmall liquid droplets on solid surfaces: production, imaging, and relevance for current wetting research. *small*, 2009. 5(12): p. 1366-1390.

8. Promraksa, A., Y.-C. Chuang, and L.-J. Chen, Study on the wetting transition of a liquid droplet sitting on a square-array cosine wave-like patterned surface. *Journal of colloid and interface science*, 2014. 418: p. 8-19.
9. Quéré, D., Wetting and roughness. *Annu. Rev. Mater. Res.*, 2008. 38: p. 71-99.
10. Shome, A., et al., Role of chemistry in bio-inspired liquid wettability. *Chemical Society Reviews*, 2022. 51(13): p. 5452-5497.
11. Wu, Y., et al., Equilibrium droplet shapes on chemically patterned surfaces: theoretical calculation, phase-field simulation, and experiments. *Journal of Colloid and Interface Science*, 2022. 606: p. 1077-1086.
12. Corti, D.S., K.J. Kerr, and K. Torabi, On the interfacial thermodynamics of nanoscale droplets and bubbles. *The Journal of chemical physics*, 2011. 135(2).
13. Wu, Y., et al., Digital twin of a droplet microarray platform: Evaporation behavior for multiple droplets on patterned chips for cell culture. *Droplet*, 2024. 3(1): p. e94.
14. Yu, D.I., et al., Dynamics of contact line depinning during droplet evaporation based on thermodynamics. *Langmuir*, 2015. 31(6): p. 1950-1957.
15. Feng, W., E. Ueda, and P.A. Levkin, Droplet microarrays: from surface patterning to high-throughput applications. *Advanced materials*, 2018. 30(20): p. 1706111.
16. Lei, W., et al., Droplet Microarray as a Powerful Platform for Seeking New Antibiotics Against Multidrug-Resistant Bacteria. *Advanced Biology*, 2022. 6(12): p. 2200166.

17. Popova, A.A., et al., Droplet-microarray on superhydrophobic–superhydrophilic patterns for high-throughput live cell screenings. *Rsc Advances*, 2016. 6(44): p. 38263-38276.
18. Shi, J., et al., A fluorescence turn-on biosensor based on graphene quantum dots (GQDs) and molybdenum disulfide (MoS<sub>2</sub>) nanosheets for epithelial cell adhesion molecule (EpCAM) detection. *Biosensors and Bioelectronics*, 2017. 93: p. 182-188.
19. Wu, H., et al., High-throughput generation of durable droplet arrays for single-cell encapsulation, culture, and monitoring. *Analytical chemistry*, 2018. 90(7): p. 4303-4309.
20. Xu, J.-G., et al., Forming a large-scale droplet array in a microcage array chip for high-throughput screening. *Analytical chemistry*, 2019. 91(16): p. 10757-10763.
21. Yu-Yao, W., et al., Advances in microdroplet generation methods. *Chinese Journal of Analytical Chemistry*, 2019. 47(6): p. 795-804.
22. Zhu, Y., et al., Sequential operation droplet array: an automated microfluidic platform for picoliter-scale liquid handling, analysis, and screening. *Analytical chemistry*, 2013. 85(14): p. 6723-6731.
23. Du, L., H. Liu, and J. Zhou, Picoliter droplet array based on bioinspired microholes for in situ single-cell analysis. *Microsystems & nanoengineering*, 2020. 6(1): p. 33.
24. Flaim, C.J., S. Chien, and S.N. Bhatia, An extracellular matrix microarray for probing cellular differentiation. *Nature methods*, 2005. 2(2): p. 119-125.

25. Iino, R., et al., Design of a large-scale femtoliter droplet array for single-cell analysis of drug-tolerant and drug-resistant bacteria. *Frontiers in Microbiology*, 2013. 4: p. 46870.
26. Tronser, T., et al., Droplet microarray based on patterned superhydrophobic surfaces prevents stem cell differentiation and enables high-throughput stem cell screening. *Advanced healthcare materials*, 2017. 6(23): p. 1700622.
27. Ziauddin, J. and D.M. Sabatini, Microarrays of cells expressing defined cDNAs. *Nature*, 2001. 411(6833): p. 107-110.
28. Chakraborty, S., et al., Droplet microarrays for cell culture: effect of surface properties and nanoliter culture volume on global transcriptomic landscape. *Materials Today Bio*, 2021. 11: p. 100112.
29. Chakraborty, S., et al., “Cells-to-cDNA on Chip”: Phenotypic Assessment and Gene Expression Analysis from Live Cells in Nanoliter Volumes Using Droplet Microarrays. *Advanced Healthcare Materials*, 2022. 11(12): p. 2102493.
30. Neto, A., P. Levkin, and J. Mano, Patterned superhydrophobic surfaces to process and characterize biomaterials and 3D cell culture. *Materials Horizons*, 2018. 5(3): p. 379-393.
31. Wang, Z., et al., High-Performance Pressure Sensors Based on Shaped Gel Droplet Arrays. *Small*, 2024. 20(5): p. 2305214.
32. Maitra, A., et al., The Human MitoChip: a high-throughput sequencing microarray for mitochondrial mutation detection. *Genome research*, 2004. 14(5): p. 812-819.

33. Zhu, Y., et al., Printing 2-dimensional droplet array for single-cell reverse transcription quantitative PCR assay with a microfluidic robot. *Scientific reports*, 2015. 5(1): p. 9551.
34. Deng, X., H. Li, and Y. Song, Inkjet printing-based high-throughput DNA synthesis. *Giant*, 2023: p. 100222.
35. Song, H., D.L. Chen, and R.F. Ismagilov, Reactions in droplets in microfluidic channels. *Angewandte chemie international edition*, 2006. 45(44): p. 7336-7356.
36. Wang, Z., et al., Optical virtual imaging at 50 nm lateral resolution with a white-light nanoscope. *Nature communications*, 2011. 2(1): p. 218.
37. Chen, Y., et al., Reducing optical losses in organic solar cells using microlens arrays: theoretical and experimental investigation of microlens dimensions. *Physical Chemistry Chemical Physics*, 2015. 17(5): p. 3723-3730.
38. Li, M., et al., Functional femtoliter droplets for ultrafast nanoextraction and supersensitive online microanalysis. *Small*, 2019. 15(1): p. 1804683.
39. Wei, Z., et al., In-situ fabrication of metal oxide nanocaps based on biphasic reactions with surface nanodroplets. *Journal of colloid and interface science*, 2022. 608: p. 2235-2245.
40. Yu, H., et al., Formation of Surface Protic Ionic Liquid Nanodroplets for Nanofabrication. *Advanced Materials Interfaces*, 2020. 7(4): p. 1901647.
41. Du, G.-S., et al., Cell-based drug combination screening with a microfluidic droplet array system. *Analytical chemistry*, 2013. 85(14): p. 6740-6747.
42. Farshchian, B., et al., Laser-induced superhydrophobic grid patterns on PDMS for droplet arrays formation. *Applied Surface Science*, 2017. 396: p. 359-365.

43. Jackman, R.J., et al., Fabricating large arrays of microwells with arbitrary dimensions and filling them using discontinuous dewetting. *Analytical chemistry*, 1998. 70(11): p. 2280-2287.
44. Jokinen, V., L. Sainiemi, and S. Franssila, Complex droplets on chemically modified silicon nanograss. *Advanced Materials*, 2008. 20(18): p. 3453-3456.
45. Ueda, E. and P.A. Levkin, Emerging applications of superhydrophilic-superhydrophobic micropatterns. *Advanced Materials*, 2013. 25(9): p. 1234-1247.
46. Awashra, M., et al., Superhydrophilic/superhydrophobic droplet microarrays of low surface tension biofluids for nucleic acid detection. *Advanced Materials Interfaces*, 2024. 11(1): p. 2300596.
47. Kobaku, S.P., et al., Patterned Superomniphobic–Superomniphilic Surfaces: Templates for Site-Selective Self-Assembly. 2012.
48. PR, K.S., et al., Wettability Engendered Templated Self-assembly (WETS) for Fabricating Multiphasic Particles. 2015.
49. Ahmed, N., et al., LBM of aluminum alloy: towards a control of material removal and roughness. *The International Journal of Advanced Manufacturing Technology*, 2019. 105: p. 1901-1915.
50. Vora, H.D. and N.B. Dahotre, Surface topography in three-dimensional laser machining of structural alumina. *Journal of Manufacturing Processes*, 2015. 19: p. 49-58.
51. Tran, N.G. and D.-M. Chun, Green manufacturing of extreme wettability contrast surfaces with superhydrophilic and superhydrophobic patterns on aluminum. *Journal of Materials Processing Technology*, 2021. 297: p. 117245.

52. Tseng, S.-F. and C.-H. Liao, Investigation of interactions between ultrafast laser beams and screen-printed silver nanopaste films. *Applied Surface Science*, 2020. 512: p. 144696.
53. Long, J., et al., Superhydrophobic surfaces fabricated by femtosecond laser with tunable water adhesion: from lotus leaf to rose petal. *ACS applied materials & interfaces*, 2015. 7(18): p. 9858-9865.
54. Vanithakumari, S., et al., Laser patterned titanium surfaces with superior antibiofouling, superhydrophobicity, self-cleaning and durability: Role of line spacing. *Surface and Coatings Technology*, 2021. 418: p. 127257.
55. Lai, F., et al., Three-dimension hierarchical Al<sub>2</sub>O<sub>3</sub> nanosheets wrapped LiMn<sub>2</sub>O<sub>4</sub> with enhanced cycling stability as cathode material for lithium ion batteries. *ACS applied materials & interfaces*, 2016. 8(33): p. 21656-21665.
56. Tran, N.G., D.-M. Chun, and A. Abd-Elrahim, Superhydrophobic aluminum surfaces with nano-micro hierarchical composite structures: A novel and sustainable approach to corrosion protection. *Journal of Alloys and Compounds*, 2023. 960: p. 170907.
57. Zhang, H., et al., Synthesis of nanostructured  $\gamma$ -AlOOH and its accelerating behavior on the thermal decomposition of AP. *RSC advances*, 2016. 6(32): p. 27235-27241.
58. Pletincx, S., et al., In situ characterization of the initial effect of water on molecular interactions at the interface of organic/inorganic hybrid systems. *Scientific reports*, 2017. 7(1): p. 45123.



59. Tran, N.G. and D.-M. Chun, Simple and fast surface modification of nanosecond-pulse laser-textured stainless steel for robust superhydrophobic surfaces. *CIRP Annals*, 2020. 69(1): p. 525-528.
60. Ngo, C.-V. and D.-M. Chun, Control of laser-ablated aluminum surface wettability to superhydrophobic or superhydrophilic through simple heat treatment or water boiling post-processing. *Applied Surface Science*, 2018. 435: p. 974-982.
61. Strålin, A. and T. Hjertberg, Influence of surface composition on initial hydration of aluminium in boiling water. *Applied surface science*, 1994. 74(3): p. 263-275.